OPTIMIZING THE DESIGN OF INFILTRATION TRENCHES FOR STORMWATER RECHARGE IN HARRIS COUNTY, TEXAS

A Thesis

by

RYAN AVERY EDWARDS

Submitted to the Graduate and Professional School of
Texas A&M University
in partial fulfillment of the requirements for the degree of

MASTER OF SCIENCE

Chair of Committee,	Gretchen R. Miller
Committee Members,	Francisco Olivera
	Salvatore Calabrese
Head of Department,	Zachary Grasley

December 2022

Major Subject: Civil Engineering

ABSTRACT

Houston, Texas and Harris County, Texas are unfortunately susceptible to both flooding and drought. To alleviate problems from both of these extreme events, infiltration managed aquifer recharge (MAR) systems can be implemented. In this study, the spacing, width, and depth of rectangular parallel infiltration trenches are compared for three soil types and three water table (WT) depths to determine the resulting infiltration rates. Analysis was conducted using two-dimensional numerical simulations with the HYDRUS software package.

Modeling of two groups was conducted; one varied the number of trenches in a fixed area and the other varied the width and depth of trenches while maintaining a constant trench volume. Increasing the number of trenches within a fixed area resulted in (1) increased infiltration that slightly diminished as more trenches were added and (2) an increased proportion of infiltration coming from the bottom of the trenches compared to the sides. Increasing trench width while decreasing trench depth resulted in (1) decreased infiltration and (2) an increased proportion of infiltration coming from the bottom of the trenches compared to the sides. Varying the depth to water table did not have a significant impact on the infiltration rate for most simulations in this study. However, the impact of the water table is expected be evident for smaller depths to water table. Functions were created for both modeling groups that show similar trends of infiltration rates for the three tested soil types.

ACKNOWLEDGEMENTS

I would like to thank my committee chair, Dr. Gretchen Miller, and my committee members, Dr. Francisco Olivera and Dr. Salvatore Calabrese, for their guidance, support, and patience throughout this research process.

I would also like to thank Saheli Majumdar, Santi Ramírez, and all other members of the Miller Geoecohydrology Research Group for their encouragement throughout my graduate studies.

Finally, thank you to my parents for their support and advice throughout these past few years.

CONTRIBUTORS AND FUNDING SOURCES

Contributors

This work was supervised by a thesis committee consisting of Dr. Gretchen Miller and Dr. Francisco Olivera of the Department of Civil & Environmental Engineering and Dr. Salvatore Calabrese of the Department of Biological and Agricultural Engineering.

All work for the thesis was completed independently by the student, under the advisement of Dr. Gretchen Miller.

Funding Sources

This work was also made possible in part by Harris County Flood Control District via subcontract with Binkley and Barfield, Inc. Its contents are solely the responsibility of the authors and do not necessarily represent the official views of the Harris County Flood Control District.

NOMENCLATURE

BC	Boundary condition
BMP	Best Management Practice
ENSO	El Niño/Southern Oscillation
FE	Finite Element
MAR	Managed Aquifer Recharge
SWRC	Soil-water retention curve
TWDB	Texas Water Development Board
WT	Water table
h	Pressure head [L]
K	Unsaturated hydraulic conductivity [LT^{-1}]
K_s	Saturated hydraulic conductivity [LT^{-1}]
l	Pore-connectivity parameter [-]
n	Parameter in the soil-water retention function [-]
m	Parameter in the soil-water retention function [-]
S_e	Degree of saturation [-]
α	Parameter in the soil-water retention function [L^{-1}]
θ	Water content [-]
θ_r	Residual water content [-]
θ_s	Saturated water content [-]

TABLE OF CONTENTS

Page

LIST OF FIGURES

Page

LIST OF TABLES

Page

1. INTRODUCTION

1.1. Background

The flooding risk of Houston, Texas and Harris County, Texas has recently been demonstrated by Hurricane Harvey and Tropical Storm Allison, which caused respective damages of $148.8 billion and $14.0 billion (NOAA National Centers for Environmental Information, 2022). This flooding has been exacerbated due to Houston's rapid urban growth and subsequent increased amount of land covered with concrete and asphalt (Zhang et al., 2018). Flooding is also projected to increase in strength and frequency in the future for the region due to the effects of climate change (Emanuel, 2017).

Texas also happens to be a water-stressed region that will face many future challenges from drought (Nielsen-Gammon et al., 2020). In most parts of Texas, the 1950-1957 drought was the worst drought recorded in the past 125 years of instrumental record (Nielsen-Gammon et al., 2020). In the Texas Water Development Board (TWDB) 2022 State Water Plan, this drought of record is used as the statewide benchmark for the water planning process for most of Texas. However, tree ring studies have shown that severe droughts lasting a decade or longer have occurred at least once per century in Texas (Cleaveland et al., 2011). Climate projections also predict more intense droughts in the future (Cook et al., 2019), which is concerning for the growing Texas population.

The El Niño/Southern Oscillation (ENSO) also influences extreme events in Texas. In the surrounding region, El Niño phases are linked with increased precipitation and La Niña phases are linked with decreased precipitation (Gershunov, 1998; Kurtzman

& Scanlon, 2007). Extreme ENSO events have increased in frequency over the past century (Gergis & Fowler, 2006) and are expected to become even more frequent in the future (Cai et al., 2015).

Harris County and the majority of southeast Texas is underlain by the Gulf Coast Aquifer System, which has the Chicot, Evangeline, and Jasper aquifers as its three primary aquifers (Figures 1, 2, and 3). These aquifers supply most of the water used for industrial, municipal, agricultural, and commercial purposes in the Houston metropolitan area (Kasmarek & Robinson, 2004). Unfortunately, excessive groundwater withdrawal in the region has reduced available groundwater supplies and led to land subsidence (Kearns et al., 2015).

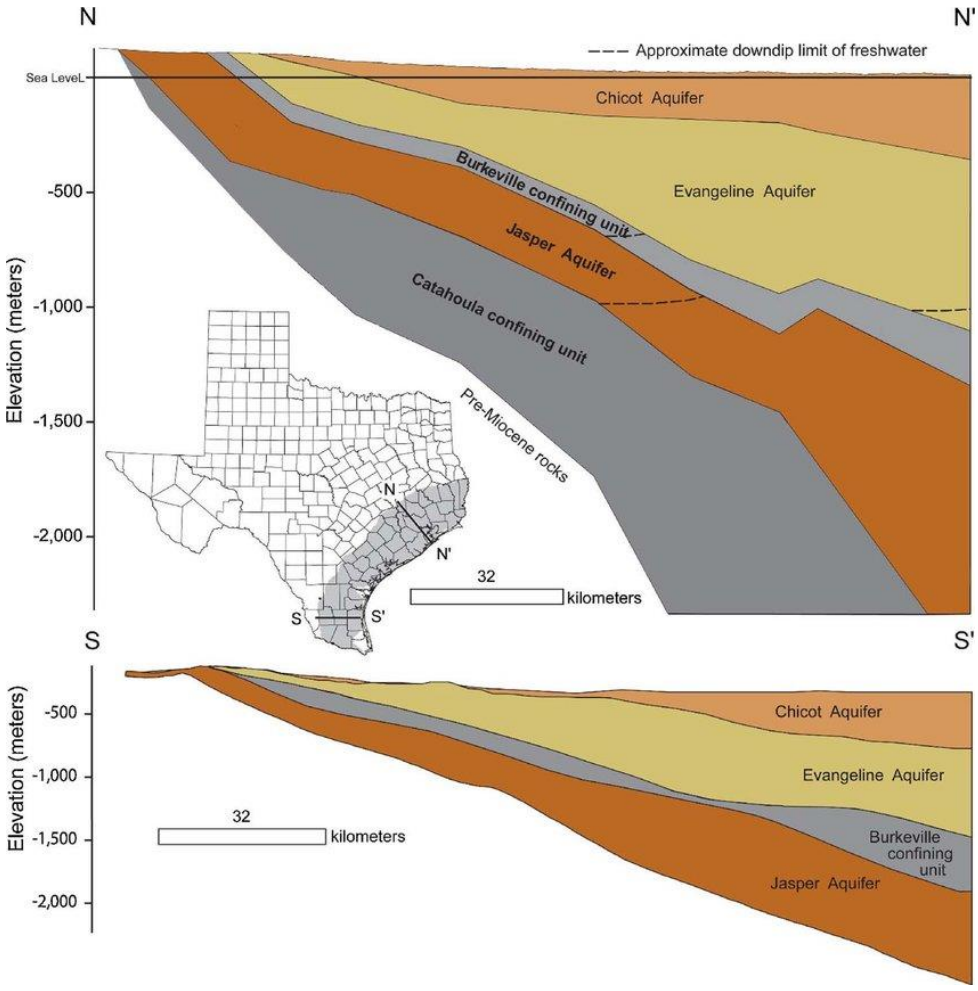

Figure 1. Hydrogeologic cross-sections of the Gulf Coast Aquifer System for the state of Texas. Cross-section N-N' is the exact same as the Figure 2 cross-section. Reprinted from Smith et al. (2017).

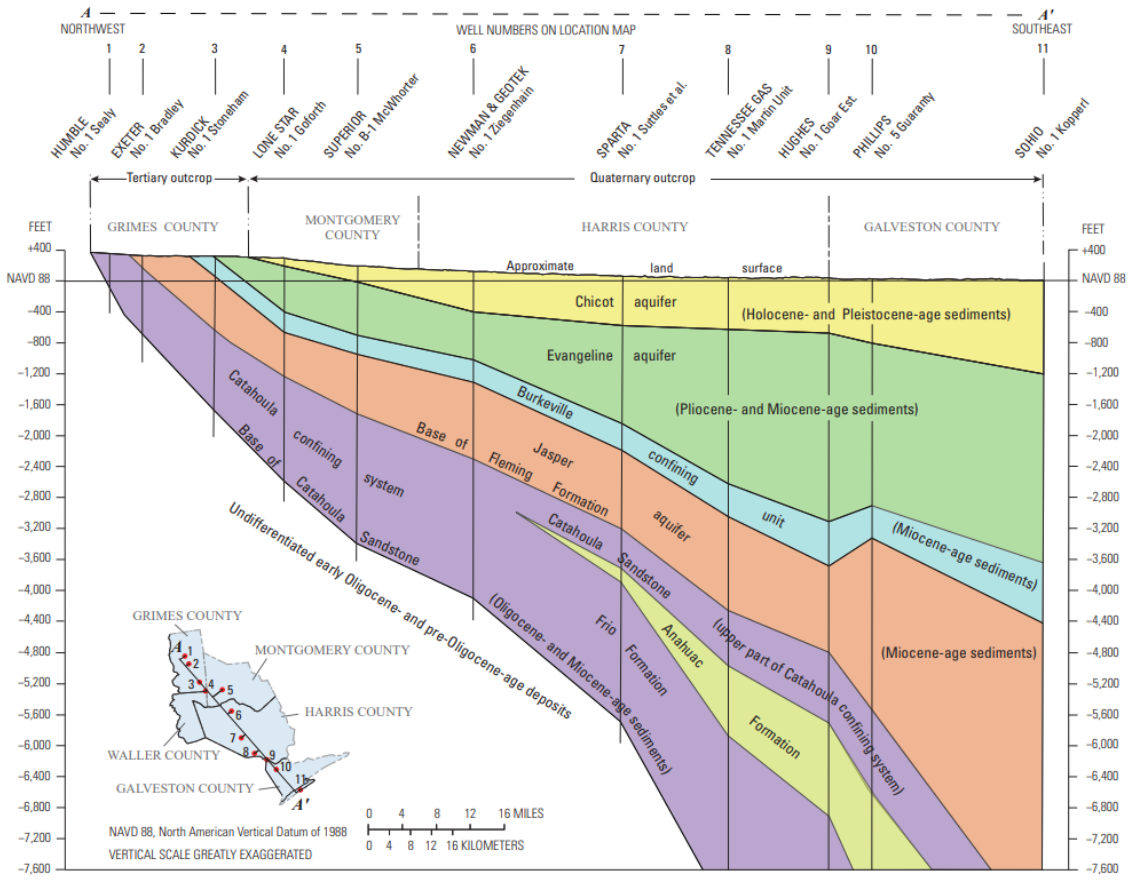

Figure 2. Hydrogeologic cross-section of the Gulf Coast Aquifer System. This figure shows that infiltration MAR projects in Harris County will result in recharge for the Chicot Aquifer. However, this will also impact the Evangeline Aquifer as the Chicot and Evangeline Aquifers do not have a confining unit between them and are hydraulically connected (Kearns et al., 2015). Reprinted from Braun & Ramage (2020).

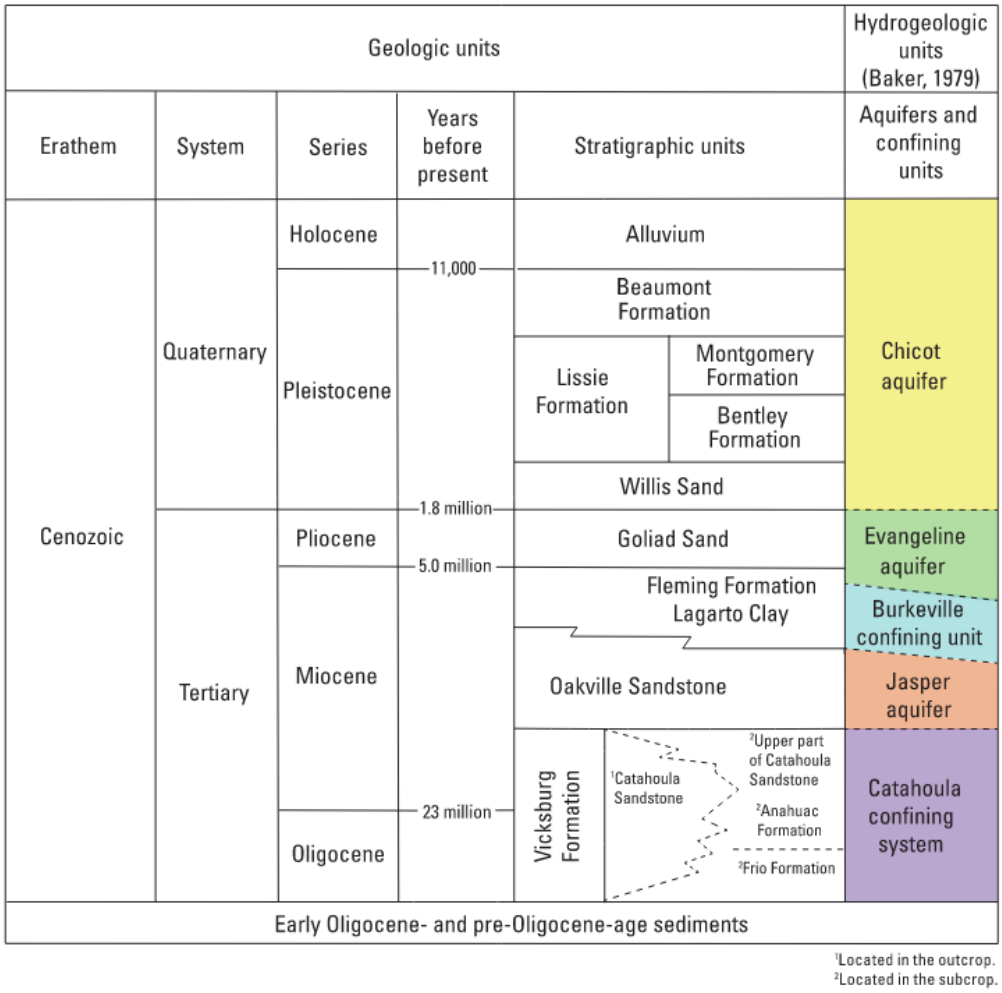

Figure 3. Geologic and hydrogeologic units of the Gulf Coast Aquifer System in the Houston-Galveston region. Reprinted from Braun & Ramage (2020).

Land subsidence reduces aquifer storage, causes structural damage and wetland loss, and leads to increased flooding (Coplin & Galloway, 1999; Kearns et al., 2015). Much of central to southeast Harris County has subsided by at least 6 ft (Kasmarek, 2013), which was mostly the result of municipal and industrial withdrawals in between the 1940s and 1960s (Kearns et al., 2015). This led to the creation of the Harris-Galveston Subsidence District in 1975 in order to regulate and reduce groundwater

withdrawals (Braun & Ramage, 2020). A study by Miller & Shirzaei (2019) found that 85 percent of the flooded area from Hurricane Harvey in Houston and Galveston had subsided at a rate over 5 mm/yr, which shows a strong correlation between flooding and subsidence.

The 2022 Texas State Water Plan from the TWDB projects the state population to increase from 29.7 million in 2020 to 51.5 million in 2070, which is a 73 percent increase. Climate change is also expected to increase the frequency and intensity of both flooding (Emanuel, 2017) and droughts (Nielsen-Gammon et al., 2020). To account for these problems, infiltration MAR structures can be implemented.

1.2. Literature Review

Infiltration MAR structures aim to reduce flooding and store additional water as groundwater. This then increases water availability during drought and reduces potential land subsidence and saltwater intrusion. These structures work by introducing more permeable materials and/or diverting water to increase the infiltrating area. Some examples of infiltration MAR structures are infiltration trenches, infiltration basins, infiltration galleries, dry (vadose zone) wells, and channel spreading (Maliva, 2020).

Stormwater infiltration trenches are long, narrow pits that are filled with sand, stone, or gravel to collect and infiltrate stormwater. They are often dug with a backhoe and are typically sized to less than 1 m wide and 5 m deep (Bouwer, 2002). Trenches are lined with a geotextile filter cloth and can also include a topsoil layer and perforated pipe underdrains (Duchene et al., 1994). They are typically used as a stormwater best management practice (BMP) to collect runoff from small drainage areas such as parking

lots (Chahar et al., 2012). This is different than this study, which simulates rows of infiltration trenches for larger drainage areas instead of single trenches for small drainage areas.

Stormwater infiltration structures are sized differently based upon the desired goals of the structure. When designed as a BMP, trenches are typically sized to either prioritize storage or water quality (Schueler, 1987). When storage is the main priority, the trenches are sized based upon a design storm and its corresponding capture volume and storage time (Akan, 2002). When water quality is the priority, trenches are sized to contain the first flush of runoff and typically have water quality volumes based upon 25- or 50-mm design storms (Schueler, 1987; Guo & Gao, 2016). This study also takes a different approach towards sizing infiltration trenches, as the goal of this study is to maximize infiltration rather than fit a required amount of water.

In order for infiltration structures to be feasible in an area, the soil must have adequate permeability and the existing water table and confining layers must be sufficiently low (Akan, 2002). In a study on groundwater interference for infiltration trenches, Locatelli et al. (2015) determined that trench performance is affected for unsaturated depths of less than 1.5 to 3 m in sandy loam, 6.5 to 8 m in silt loam and 11 to 12 m in silty clay loam. Locatelli et al. (2015) also recommends that trenches not be constructed for soils with a hydraulic conductivity on the order of 1 x 10-7 m/s or lower due to the required large storage volumes associated. Infiltration structures should also not be constructed in soils with high clay contents, such as 30 percent as recommended by the Virginia Department of Transportation (2013).

Clogging in infiltration structures is a significant problem that can lead to reduced infiltration rates and overall failure of the system. Clogging can be caused by a variety of physical, chemical, and biological processes that reduce soil permeability and porosity (Baveye et al., 1998). Some examples include deposition of suspended solids, formation of biofilms, precipitation of salts, and formation of entrapped gases in the soil (Bouwer, 2002). However, deposition of suspended sediments is the primary cause of clogging for stormwater infiltration structures (Siriwardene et al., 2007).

Pretreatment and/or erosion control are used in infiltration systems to mitigate the effects of clogging and improve the water quality of infiltrating stormwater. Some examples of pretreatment methods typically used for stormwater BMPs are sediment forebays, vegetated buffer strips, and presettling basins (Maniquiz-Redillas et al., 2014). Pretreatment is especially necessary for infiltration MAR projects because of the large amounts of suspended solids and sediment in stormwater. Pretreatment was not included in the site of the previous two-year study (Albert et al., 2021), as clogging was not its main focus. However, future infiltration projects that are constructed in detention basins could require pretreatment.

When designing infiltration structures, the costs of inspection, operation, and maintenance should be considered (Maliva, 2020). In a survey of Maryland infiltration BMPs, Lindsey et al. (1992) found that 53 percent of the surveyed infiltration trenches were functioning as designed and 73 percent required maintenance. The main mode of failure for these trenches in the survey was due to sedimentation, which inspectors noted as often accelerated by inadequate vegetated buffer strips.

Many analytical and empirical equations have been developed to estimate infiltration from the bottom and sides of infiltration trenches (Bouwer, 2002; Campisano et al., 2011; Chahar et al., 2012; Guo & Gao, 2016; Wang & Guo, 2020). These equations are typically used to size single infiltration trenches for a particular design storm. However, there is a lack of research that is focused on estimating the infiltration of multi-trench systems.

Heilweil et al. (2014) used a variably saturated flow model to compare the relative importance of trench variables for infiltration performance in a multi-trench system. This modeling showed that "deeper and wider trenches do not substantially increase infiltration" and "larger numbers of parallel trenches within a fixed area increases infiltration but with a diminishing effect as trench spacing becomes tighter" (Heilweil et al., 2014). These results suggest that there may be an optimal trench configuration (dimensions and spacing) for a particular location and set amount of infill.

1.3. Previous Study

This synthetic case study builds upon a previous study from Albert et al. (2021), who evaluated three different infiltration MAR methods in an existing detention basin in northwest Harris County. In the previous study, three 30.48 m by 30.48 m plots were constructed with each infiltration method and tested against a control plot. These plots were then monitored for two years to assess the corresponding recharge performance. The plot with 16 rectangular infiltration trenches (Figure 4) is the focus of this study.

The 16 infiltration trenches in the previous study from Albert et al. (2021) had a width of 61.0 cm, a depth of 91.4 cm, and a length of 30.48 m. The spacing between the

center lines of each trench was 182.9 cm, which creates a 121.92 cm gap between each trench (Figure 4). The upper 15.2 cm of the trenches were filled with type #57 limestone gravel (<5 cm diameter) and the lower 76.2 cm was filled with a larger recycled concrete aggregate (Figure 5). Over the two-year period, the cumulative infiltration was 61%, or 127 cm, greater for the trench plot versus the control plot. However, this infiltration could have potentially been improved given a different trench geometry and/or spacing.

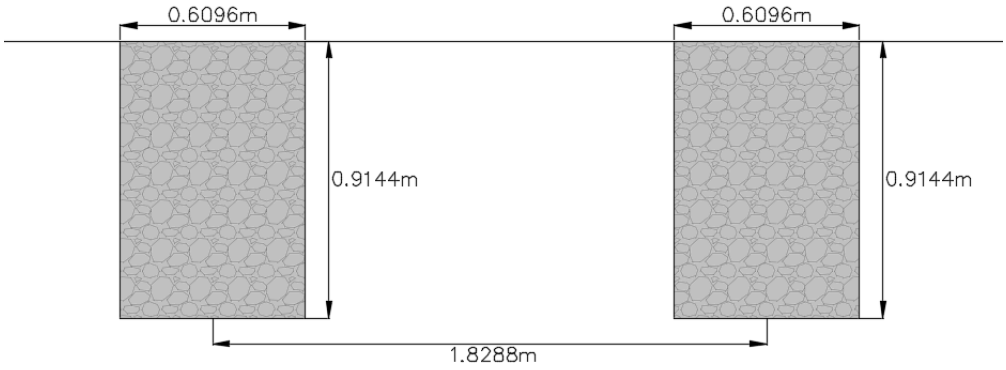

Figure 4. Trench cross-sections for the previous Albert et al. (2021) study. For the purposes of this study, the trenches were assumed to be one gravel type instead of the two types shown in Figure 5.

Figure 5. Installation of the trench system (left) highlighting the trench fill and non-woven geotextile fabric (right). Reprinted from Albert et al. (2021).

1.4. Objectives

The main objective of this study is to use vadose zone numerical modeling to test how changing trench spacing, width, and depth affects the infiltration rate of a plot of parallel infiltration trenches in a detention basin. Two-dimensional numerical simulations were conducted for each different configuration using the HYDRUS-2D software package (Šimůnek et al., 2020). Simulations were also performed for different soil types (loam, sandy loam, and silty loam) and initial depths to water table (10 m, 15 m, and 20 m) in order to evaluate the relative importance of these variables. The amount of infiltration leaving the bottom and sides of the trenches was also determined to obtain a proportion for each simulation.

2. METHODOLOGY AND MODELING

2.1. Governing Equations

The HYDRUS-2D software package is used in this research to numerically solve the Richard's equation for water movement in variably saturated porous media (Šimůnek et al., 2020). HYDRUS allows users to choose between different soil hydraulic models; for this research, the van Genuchten-Mualem model was selected (van Genuchten, 1980; Mualem, 1976). The expressions are given by:

$$\theta(h) = \begin{cases} \theta_r + \dfrac{\theta_s - \theta_r}{(1 + |\alpha h|^n)^m} & h < 0 \\ \theta_s & h \geq 0 \end{cases}$$

$$K(h) = K_s S_e^l \left[1 - \left(1 - S_e^{1/m}\right)^m\right]^2$$

$$S_e = \frac{\theta - \theta_r}{\theta_s - \theta_r}$$

where, θ is soil-water content, θ_s and θ_r are saturated and residual soil-water contents, h is pressure head, α, n, and m are characterizing parameters for a given soil, K is unsaturated hydraulic conductivity, K_s is saturated hydraulic conductivity, S_e is degree of saturation, and l is the pore-connectivity parameter for a given soil (Šimůnek et al., 2020). In this model, m and n are related by the following relationship from van Genuchten (1980):

$$m = 1 - 1/n$$

2.2. Soil Types

Loam, silty loam, and sandy loam were selected as representative soil types to test for the simulations. These three soil types were the most common textural classifications from the site of the previous study (Albert et al., 2021). The percentages for the dominant soil textures in Harris County, Texas (Table 1) were also obtained from the Web Soil Survey from the Natural Resources Conservation Service (2022). Although clay and clay loam were the second and fourth most common in Table 1, they were not selected to model due to the lower clay content that is necessary for infiltration structures.

Table 1. Surface soil type percentages for Harris County, Texas

Soil type	Percentage
Fine sandy loam	36.5
Clay	19.9
Loam	15.1
Clay loam	10.4
Silt loam	4.3
Very fine sandy loam	2.6
Silty clay loam	2.0
Loamy fine sand	1.6
Silty clay	0.5
Fine sand	0.4
Other	6.7

2.3. Soil Hydraulic Parameters

The van Genuchten parameters and saturated hydraulic conductivities for loam, silty loam, and sandy loam (Table 2) were obtained from the ROSETTA program (Schaap et al., 2021) that is implemented into HYDRUS (Šejna et al., 2014). The ROSETTA program estimates soil hydraulic parameters using pedotransfer functions and a large dataset of soil samples (Schaap et al., 2021). The default parameters based

upon textural classes in ROSETTA were selected in this study. The pore-connectivity parameter *l* was set as 0.5 for all soil types based upon the study by (Mualem, 1976). Figure 6 shows the plotted van Genuchten soil-water retention curves for the soil types used in this study.

Table 2. Soil Hydraulic Parameters

Soil type	θ_r [cm^3/cm^3]	θ_s [cm^3/cm^3]	α [1/m]	n [-]	K_s [cm/day]	l [-]
Loam	0.0609	0.3991	1.11	1.4737	12.04	0.5
Sandy Loam	0.0387	0.3870	2.67	1.4484	38.25	0.5
Silty Loam	0.0645	0.4387	0.51	1.6626	18.26	0.5
Gravel	0.0530	0.5070	20.00	3.0000	24,000	0.5

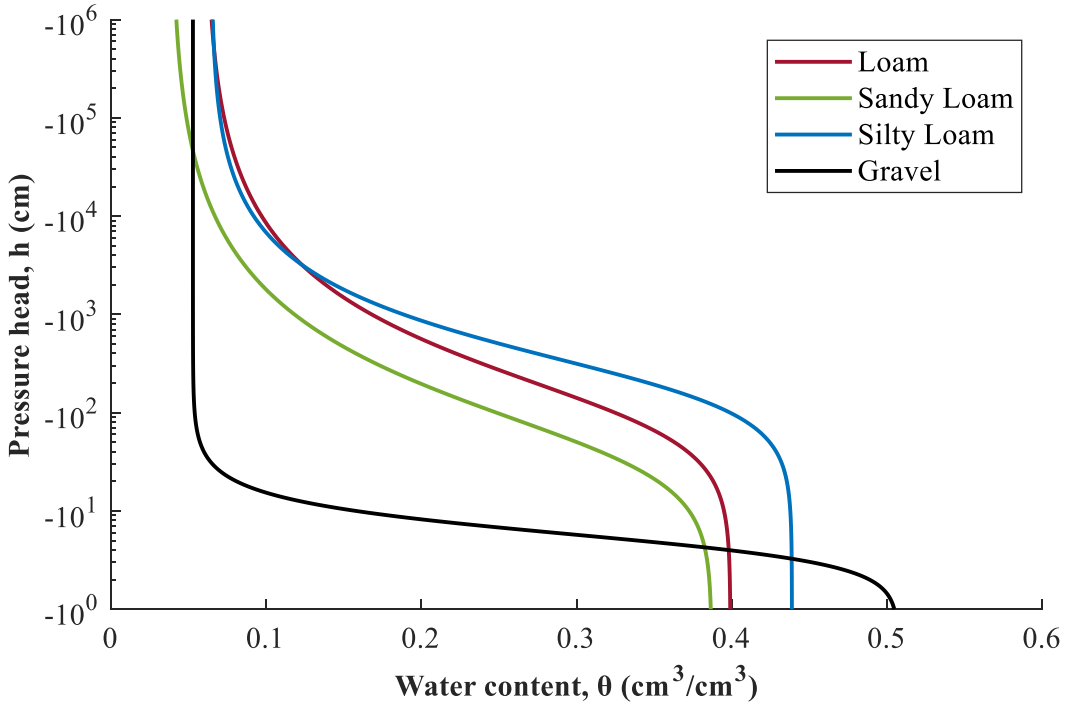

Figure 6. Soil-water retention curves using the van Genuchten (1980) model.

Determining the van Genuchten parameters and K_s for the gravel inside the trenches was more challenging. The ideal soil-water retention curve for gravel is flat and

equal to θ_r for negative matric potentials with an abrupt transition to saturation at positive pressures, which requires high α and n parameters (Finch et al., 2008). A large n parameter results in this steep curve and a large α parameter represents the small air-entry pressure of gravel. Air entry pressure (also known as bubbling pressure) is the matric suction where air starts to enter the largest pores of the soil (Wijaya et al., 2015), which is smaller for coarser soils than finer soils (Indrawan et al., 2005). Since α is inversely related to the air-entry pressure (van Genuchten, 1980), a large α is needed for gravel.

In HYDRUS, the nonlinear soil hydraulic function of gravel (as seen in Figure 6) requires finer discretization and is less numerically stable than finer-textured soils (Šimůnek & Šejna, 2009). There is not a standard range of parameters that is implemented for gravel in HYDRUS, which is likely due to the resulting instabilities. A study by Finch et al. (2008) used 175 1/m for α and 2.80 for n, which were the largest values that resulted in convergent solutions. These same parameters were also used for α and n by Błażejewski et al. (2018). A post on the HYDRUS Discussion Forums by Šimůnek (2006) recommended 20 1/m for α and 3.00 for n, which are the parameters used in this study for gravel (Table 2). A higher value for α would have been preferred, although increases led to convergence issues.

θ_r and θ_s for gravel were obtained from soil moisture sensors inside the infiltration trenches in the previous study from Albert et al. (2021). Using this soil moisture data, the smallest value was assumed to be θ_r and the largest value was assumed to be θ_s. These soil moisture contents corresponded to a long period of no

precipitation and full inundation of the infiltration trenches. Studies by Finch et al. (2008) and Błażejewski et al. (2018) used respective θ_s values of 0.50 and 0.35 and the same θ_r value of 0.05, which are close to the θ_r and θ_s values in this study (Table 2).

The saturated hydraulic conductivity K_s for gravel was set to a significantly larger value than the underlying soils. This was done in order to make the flow of water leaving the trench not be controlled by this gravel value and to ensure that the trench would fill up quickly during a precipitation event. This value is within the continuum of hydraulic conductivity ranges for well sorted gravel, which is between 0.01 and 1 cm/s (Fetter, 2018).

2.4. Modeling

2.4.1. Methodology

Two overall groups of simulations were conducted, one which varied trench spacing and another which varied trench dimensions (Tables 3 and 4). Simulations were also conducted for “full gravel” and “no gravel” cases in the trench plot in order to determine the upper and lower limits of possible infiltration for the site. The no gravel case was considered to be the control simulation to determine a baseline level of infiltration without the introduction of gravel. The full gravel simulation used the same 0.9144 m trench depth as the existing trenches, but fully covered the 15.24 m trench plot with gravel.

The full gravel simulation is the equivalent of having 50 trenches with no space between them, which showed the maximum possible infiltration that can be obtained from modifying the trench spacing. It was anticipated that as more trenches were added

to the trench plot (such as 20 and 24 trenches), the reduced space between the trenches would limit the amount of flow that is able to leave from the sides of the trenches. As a result, the simulations with 20 and 24 trenches were initially expected to approach a close value to this maximum infiltration.

These simulation groups resulted in a total of 14 different geometries, which were tested for the 3 soil types and the 3 depths to water table (10, 15, and 20 m). Each case also had 3 stages of simulations in HYDRUS, which is later described in Table 5. For each stage, the ending pressure head values for each node were imported into the following simulation as initial conditions. All of the tested variables led to a total of 378 simulations that were performed.

Table 3. Spacing Tests

Spacing (m)	Number of Trenches
1.2192	24
1.5240	20
1.8288	**16**
2.4384	12
3.0480	10
3.6576	8

Note. The bolded values are the existing trench dimensions from the Albert et al. (2021) study. The number of trenches in the models is actually half of the values in this table, as the model domain was split in half to take advantage of the symmetry.

Table 4. Dimensions Tests

Width (m)	Depth (m)	Width/Depth Ratio
0.3484	1.6002	0.2177
0.4064	1.3716	0.2963
0.4877	1.1430	0.4267
0.6096	**0.9144**	**0.6667**
0.7620	0.7315	1.0417
0.9144	0.6096	1.5000
1.0668	0.5225	2.0417

Note. The bolded values are the existing trench dimensions from the (Albert et al., 2021) study.

These 10 m, 15 m, and 20 m depths to WT were selected to be sufficiently deep to avoid full saturation of the model domain. This was due to a limitation of the software, as HYDRUS-2D runs into convergence problems when the WT reaches the surface (Šimůnek 2002). These convergence problems did occur for shallower depths to WT than 10 m, which made it the smallest that was selected. By choosing these depths to WT, the goal was to get close to seeing the impacts of the WT while still allowing the simulations to converge.

All simulations were conducted to have a water content balance error of less than 1% between time steps. Pressure head tolerance for nodes in the saturated region was set at 1 cm, which is the default. Water content tolerance for nodes in the unsaturated flow region was set at 0.0001, which was decreased from the default of 0.001 to account for the sharper transitions in the soil-water retention curve for gravel.

2.4.2. Domain

Models were constructed in HYDRUS with a horizontal domain of 100 m and a vertical domain of 40 m (Figure 7). The problem was modeled to be symmetric across the centerline of the trench plot, which is the no flow boundary condition (BC) on the

left side of Figure 7. This symmetry saved computation time, as only the right half of a 200 m total horizontal domain was modeled. This 100 m domain also only required half as many trenches to be modeled than the values listed in Table 3.

A constant head BC was set on the right side of Figure 7 that started with a pressure head of 0 m at the water table level and increased linearly with depth. This was done for the 3 simulated water tables of 10 m, 15 m, and 20 m. This constant head BC assumes that the water table outside of the model domain remains constant and forces all groundwater mounding to end at this point. This constant head BC was also the only exit point for water to leave the model domain space.

The horizontal domain of 100 m was chosen to be large enough to provide sufficient space for the groundwater mounding from the trenches, yet small enough to have feasible computation times. The configuration of trenches in Figure 7 is the same number of trenches and trench geometry of the Albert et al. (2021) study and is called the “existing trenches” for the purposes of this study. The trench variables are modified (Tables 3 and 4) only within the 15.24 m trench plot for the other simulations.

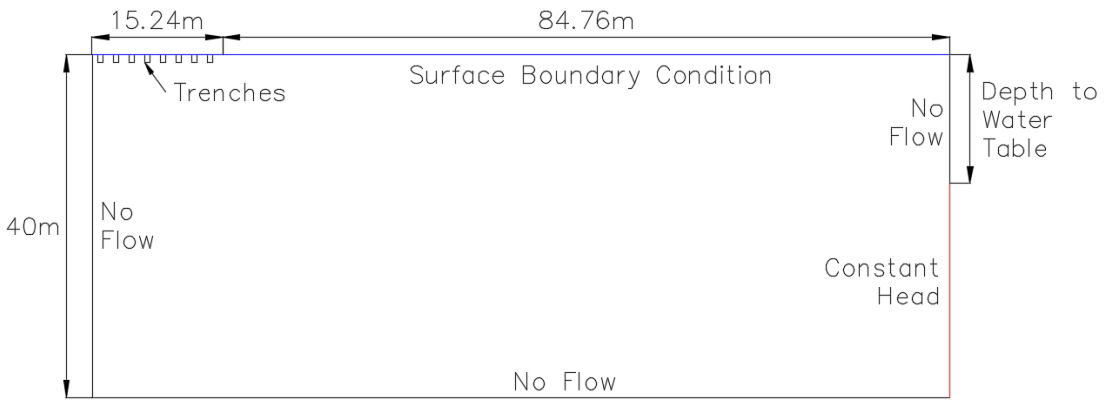

Figure 7. Conceptual model with boundary conditions and dimensions of the domain. The surface BCs change in the different simulation sections, which are shown in Table 5. Depths to WT of 10 m, 15 m, and 20 m were simulated.

2.4.3. FE Mesh

Choosing the correct spacing between elements in a finite element (FE) mesh in HYDRUS was necessary to maximize numerical accuracy while minimizing computation time. In this model, the FE mesh around surface and edges of the trenches needed to be the finer than the rest of the domain due to the larger hydraulic gradients that occur around these regions (Šimůnek & Šejna, 2009). When combined with the large domain in this model, this fine mesh requirement led to a very large number of nodes (Figure 8).

As seen in Figures 8 and 9, the FE mesh is concentrated to a size of 5 cm at the surface and around the gravel trenches. The mesh size gradually increases with depth to an eventual size of 200 cm in order to reduce computation time.

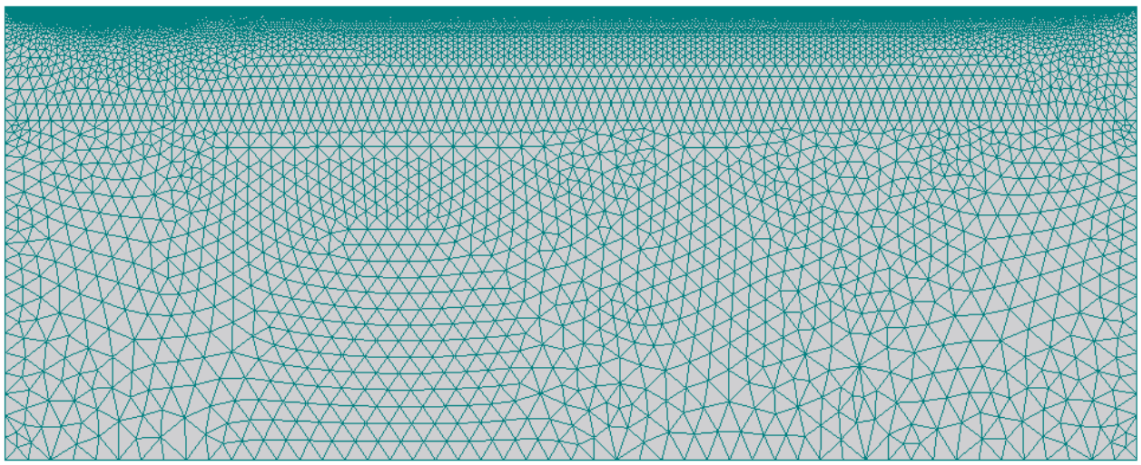

Figure 8. FE Mesh for the full domain with a total of 23,746 nodes. This figure is the trench configuration from the Albert et al. (2021) study with a 10 m depth to WT.

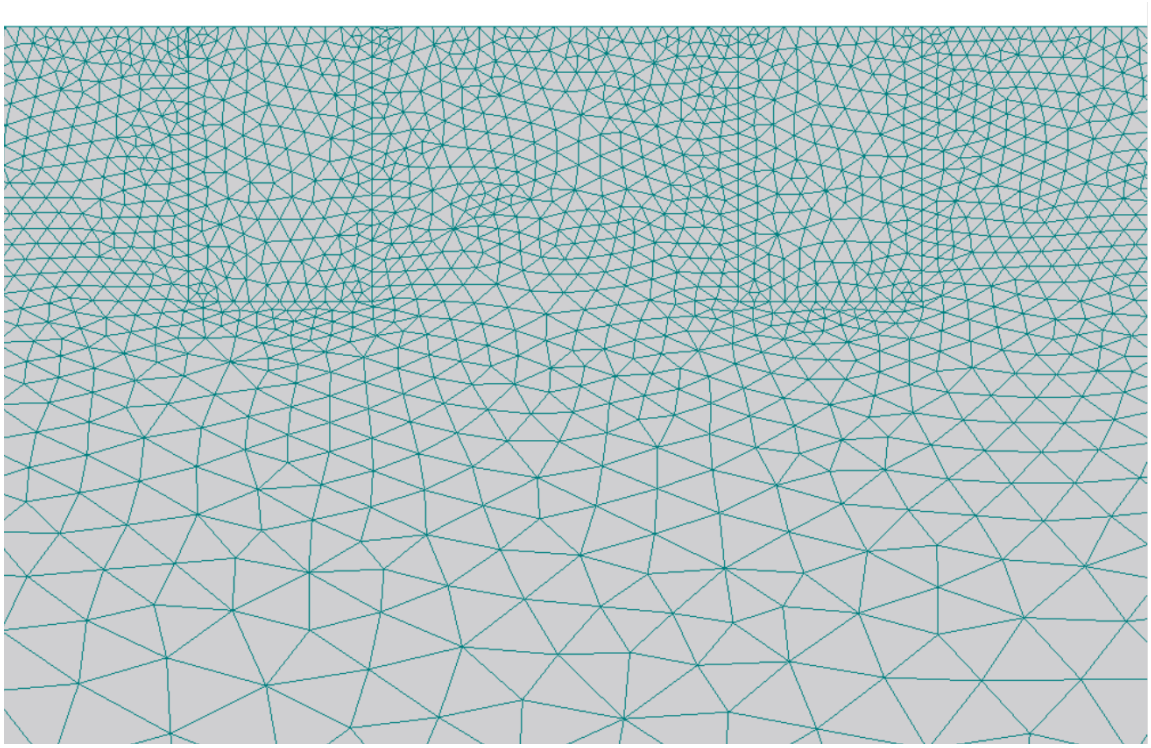

Figure 9. Zoomed in view of the FE mesh around the trenches.

2.4.4. Simulations

Simulations were conducted in 3 stages in a sequential order for each trench geometry (Table 5). This was achieved by importing the results from Group 1 into Group 2 and then Group 2 into Group 3. There were actually 4 sections that were modeled, but the Buffer and Inundation sections were able to be combined to make it 3 simulations. These could be combined because HYDRUS allowed for the coding of atmospheric and time-variable head BCs together in the same simulation. It would have been ideal to also combine the Inundation and Dissipation Sections, but convergence problems occurred when transitioning between the inundation and dissipation BCs (discussed further in Section 2.4.4.4). An overview of the length of each simulation section and its corresponding BC is also displayed in Table 5.

Table 5. Simulation Information

Section	Surface BC	Time (hours)	Simulation Number
Initialization	Constant Flux	50,000 or 52,000	1
Buffer	Atmospheric	12	2
Inundation	Time-Variable Head	48	2
Dissipation	Atmospheric	2,340	3

2.4.4.1. Initialization Section

The initialization simulations were conducted in order to obtain reasonable water content values for the initial conditions of the inundation simulations. A constant flux boundary condition of 6.8×10^{-5} m/hr was set at the surface (Figure 7), which is approximately half of the average rainfall near the site of the previous study from Albert et al. (2021). The initialization simulations for the existing trenches from the previous study were run for 50,000 hours with a pressure head initial condition that changed

linearly with depth (Figure 10). For all other trench geometries, the results (Figure 11) were inputted as new initial conditions and run for an additional 2,000 hours. This produced practically identical results for the other geometries while significantly reducing the needed computation time.

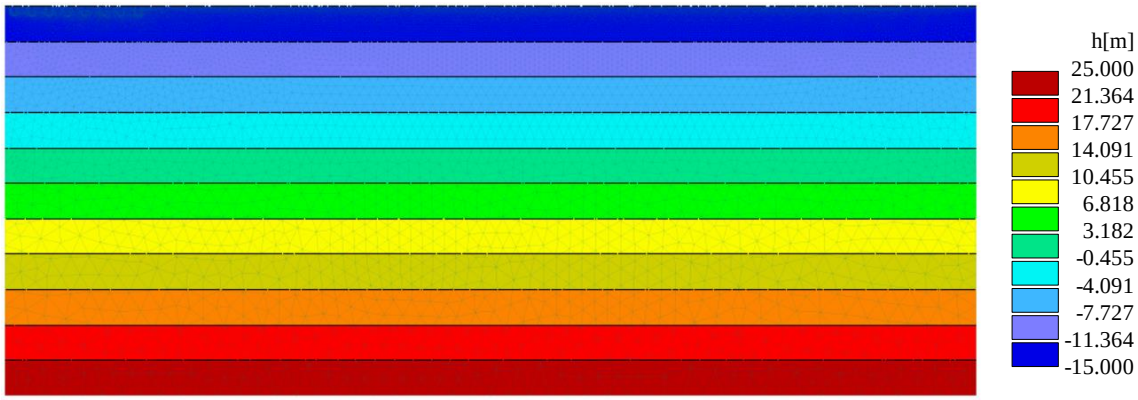

Figure 10. Pressure head initial conditions for initialization simulations for the existing trenches (15 m depth to WT).

a)

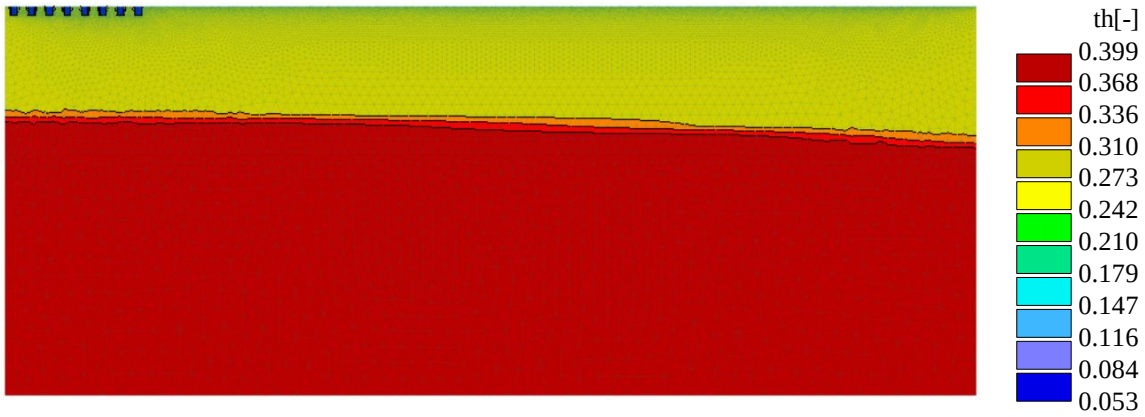

b)

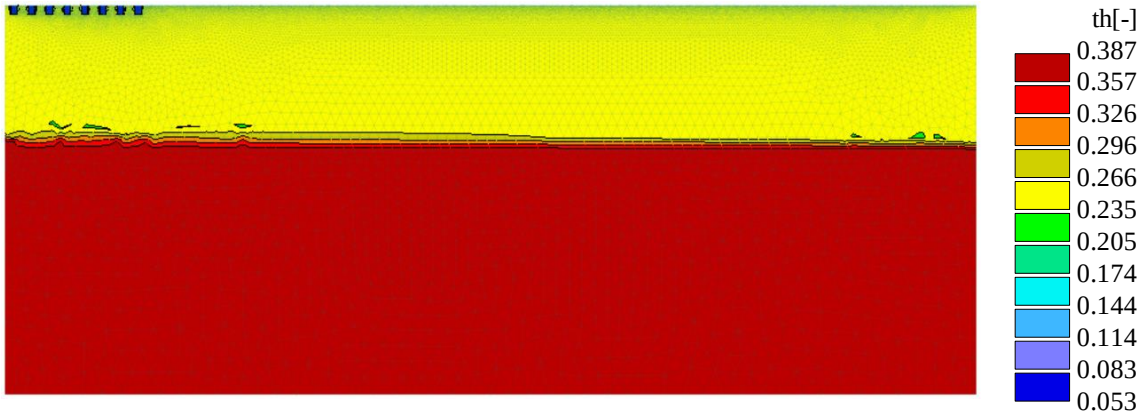

c)

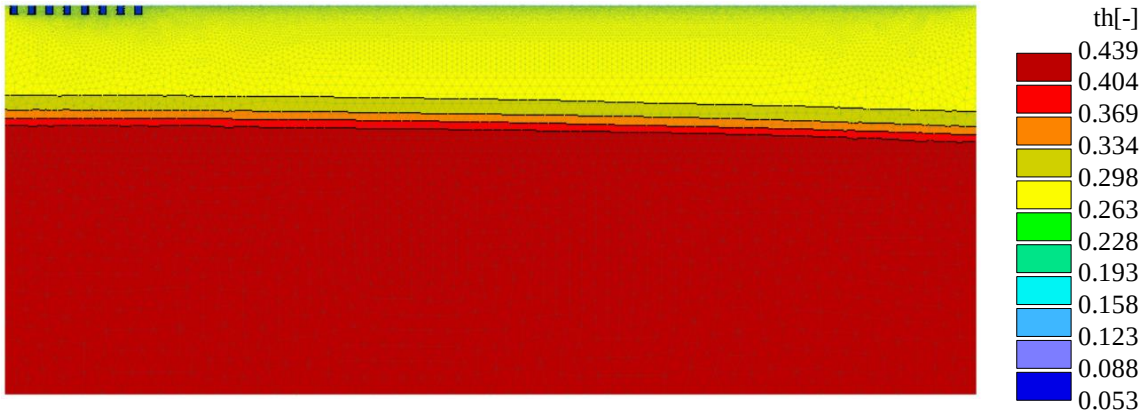

Figure 11. Water content values at end of initialization simulations for a) loam, b) sandy loam, and c) silty loam. This figure shows the simulations for the existing trenches with a 15 m depth to WT.

The initialization simulations produced approximate water contents (Figure 11) in the unsaturated zone of 0.30 for loam, 0.26 for sandy loam, and 0.28 for silty loam. Figure 11 also shows visible groundwater mounding for loam and silty loam, but not sandy loam. This is partially the result of the larger K_s for sandy loam (38.25 cm/d) than loam (12.04 cm/d) and silty loam (18.26 cm/d). Sandy loam also has a higher α parameter (2.67 1/m) than loam (1.11 1/m) and silty loam (0.51 1/m), which drops the soil-water retention curve (Figure 6). This lower curve means that sandy loam will release water at higher pressure potentials than loam and silty loam will, thus retaining less water.

2.4.4.2. Buffer Section

A "buffer" period of 12 hours with an atmospheric BC at the surface was simulated at the beginning of the second stage of simulations (Table 5). The initial conditions for this simulation group were the results from the initialization simulations (Figure 11). This section was created to prevent numerical stability problems that may have occurred when the model transitioned between the constant flux and time-variable head BCs. This section did not need to be its own simulation, as there were no problems with combining the buffer and inundation sections into one simulation.

2.4.4.3. Inundation Section

After the 12-hour buffer period, the surface BC was switched to a time-variable head BC for 48 hours. This 48-hour period was comprised of a 12-hour ramp-up period, a 24-hour constant-head period, and then a 12-hour ramp-down period. The BC pressure head for the 24-hour period was maintained at 1 m, while the BC pressure heads for the

ramp-up and ramp-down periods are shown in Table 6. The values in the ramp-up and ramp-down periods were chosen to roughly represent the shape of a hydrograph. The small values at tail end of the ramp-down period also provided a smoother transition from the time-variable BC to the atmospheric BC, which was helpful for numerical stability purposes.

Table 6. Surface boundary condition values for the 12-hour ramp-up and ramp-down periods

Time Step (hour)	Ramp-Up Pressure Head BC (m)	Ramp-Down Pressure Head BC (m)
1	0.001	0.800
2	0.005	0.600
3	0.010	0.400
4	0.025	0.300
5	0.050	0.200
6	0.100	0.150
7	0.150	0.100
8	0.200	0.050
9	0.300	0.025
10	0.400	0.010
11	0.600	0.005
12	0.800	0.001

The water contents at the end of the inundation sections are shown in Figure 13 for the existing trench geometries with a 15 m depth to WT on the right side of the model. The differences in the wetting front speeds are visible for sandy loam in Figure 13b, as it has traveled farther than loam and silty loam at the end of this section. As stated in Section 2.4.4.1, this is the result of the larger K_s and α parameters for sandy loam than loam and silty loam (Table 2). The velocity vectors are also plotted in Figure 12, which shows increasing velocities for loam, silty loam, and sandy loam, respectively.

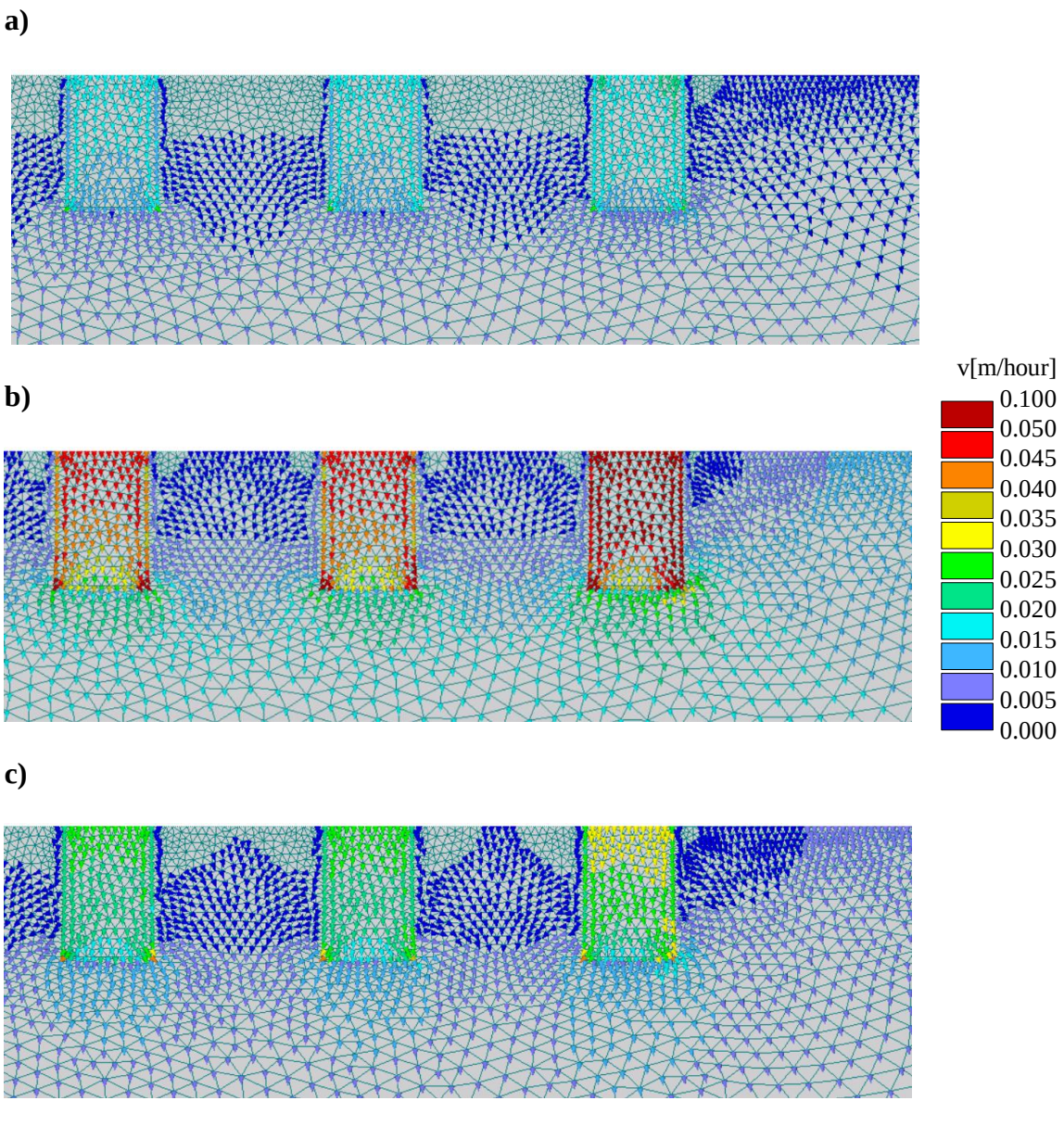

Figure 12. Velocity vectors for a) loam, b) sandy loam, and c) silty loam at the end of the inundation simulation section. This figure shows the simulations for the existing trenches with a 15 m depth to WT.

The wetting fronts for loam and silty loam traveled approximately the same distances even though the K_s of silty loam (18.26 cm/d) is larger than loam (12.04 cm/d). However, the smaller α value of silty loam (0.51 1/m) compared to loam (1.11 1/m) may

have offset the effects of these K_s differences. This smaller α value causes the SWRC (soil-water retention curve) for silty loam to be higher than loam for the portions of the curve that are closer to saturation (especially since they have similar n values) (Figure 6). These portions of the curve are also the part being simulated, as the initial conditions for this section were around 0.30 for loam, 0.26 for sandy loam, and 0.28 for silty loam in the unsaturated zone. As a result, this higher SWRC curve for silty loam means that it will retain more water for a given pressure potential than loam.

The water contents at the end of the inundation simulations for the no gravel and full gravel simulations are also displayed for loam in Figure 14. These simulation results show the wetting fronts that result from introducing no gravel and the maximum amount of gravel within the trench plot area. If the water contents from Figure 14a were to be subtracted and superimposed from Figure 13a, this would visually represent the increased infiltration from the trenches for the loam soil type.

a)

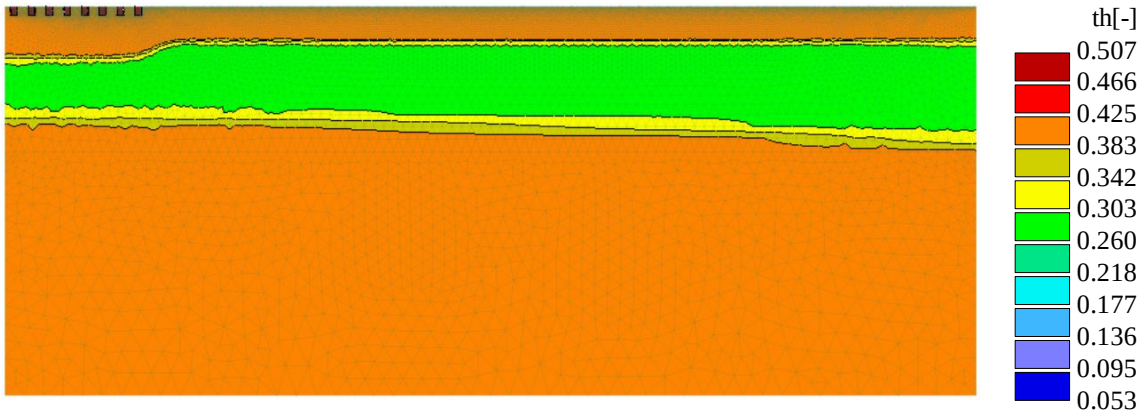

b)

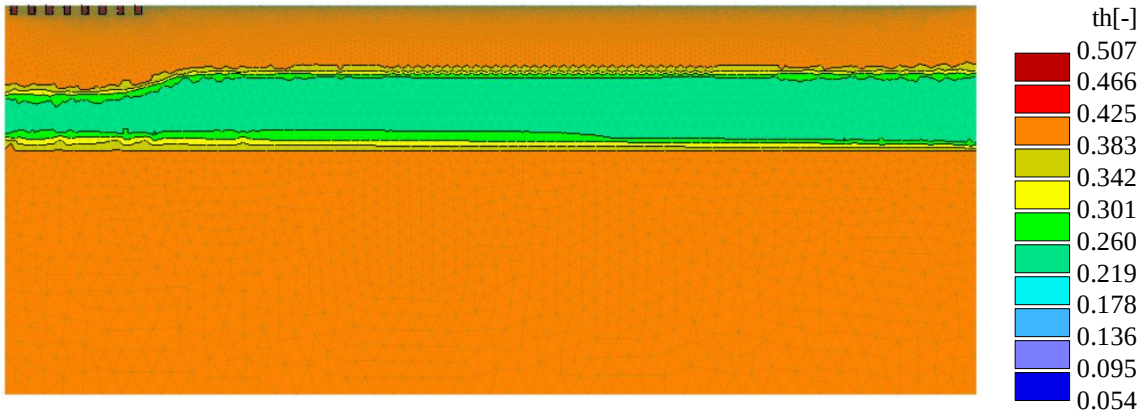

c)

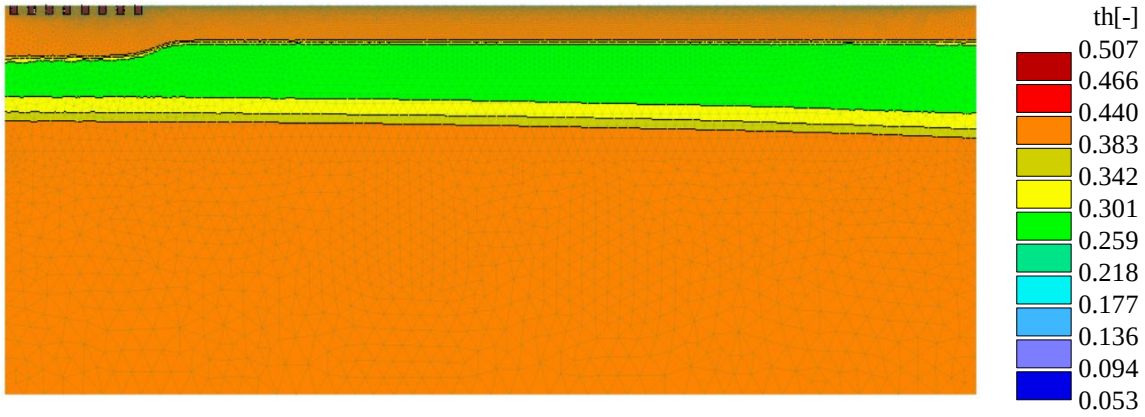

Figure 13. Water content values at end of inundation simulations for a) loam, b) sandy loam, and c) silty loam. This figure shows the simulations for the existing trenches with a 15 m depth to WT.

a)

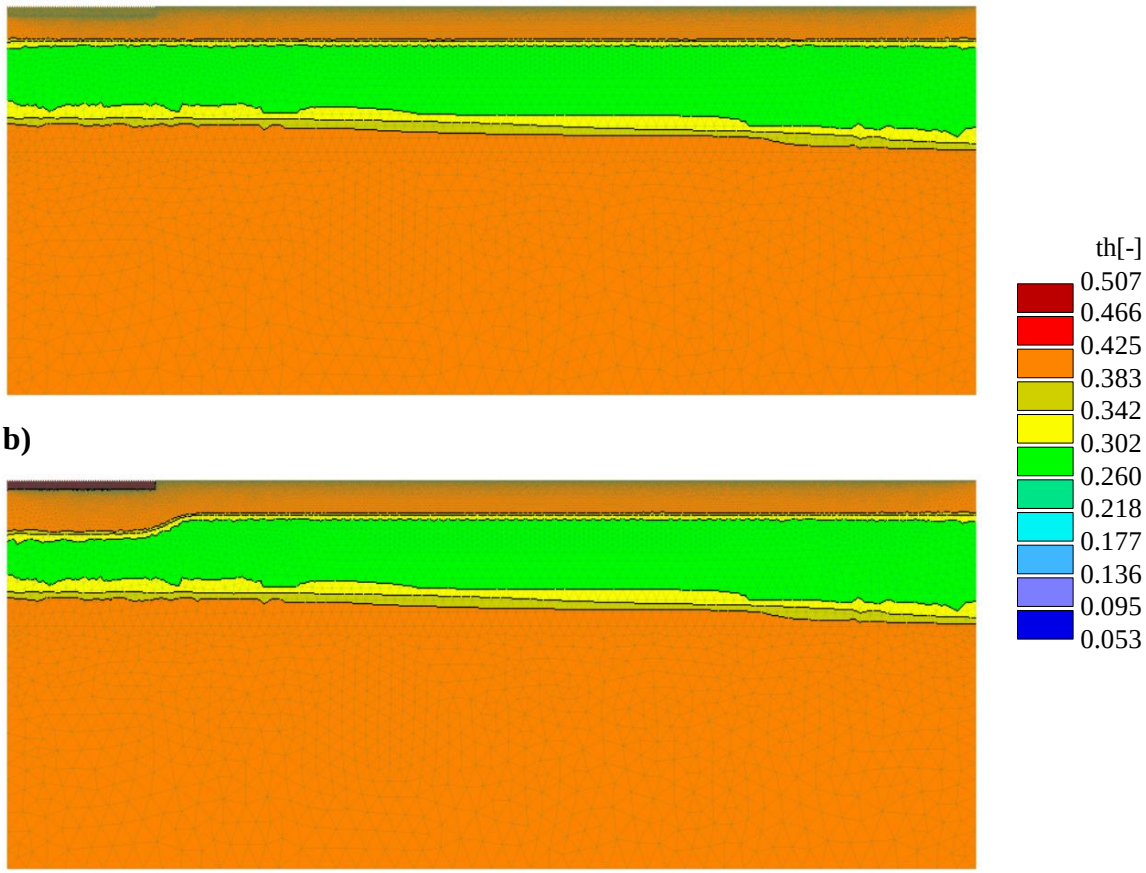

b)

Figure 14. Water content values at end of inundation simulations for the a) no gravel and b) full gravel cases. This figure shows the simulations for the loam soil type and a 15 m depth to WT.

2.4.4.4. Dissipation Section

In this final modeling section, the surface BC was switched back to an atmospheric BC and the simulation was run for 2,340 hours (Figure 15). This provided enough time for the wetting fronts for all of the simulations to dissipate. The system did not fully reach equilibrium in this section due to the slow nature of groundwater movement, but that was not necessary for the goals of this study.

The dissipation section needed to be its own simulation group, as the switch to the atmospheric BC caused the simulation to not converge when too much of the area close to the surface was fully saturated. This was similar to the convergence issues that occur when the WT reaches the surface (discussed in Section 2.4.1). However, this did not occur for the tested depths to WT for this study (Figure 13).

To achieve convergence, the uppermost nodes on the surface were set as very slightly unsaturated (as close as possible) for the initial conditions of this section. Initial condition pressure heads of -0.01 m for sandy loam and -0.001 m for loam and silty loam were set. This decreased the respective water contents of loam, sandy loam, and silty loam by 5.0×10^{-5}, 5.7×10^{-4}, and 1.0×10^{-5}, all of which are not a significant change from the saturated water contents.

a)

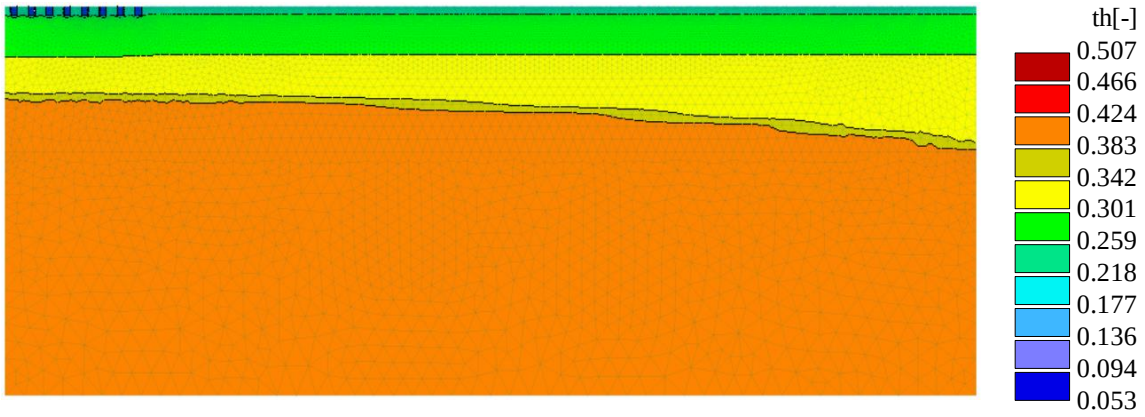

b)

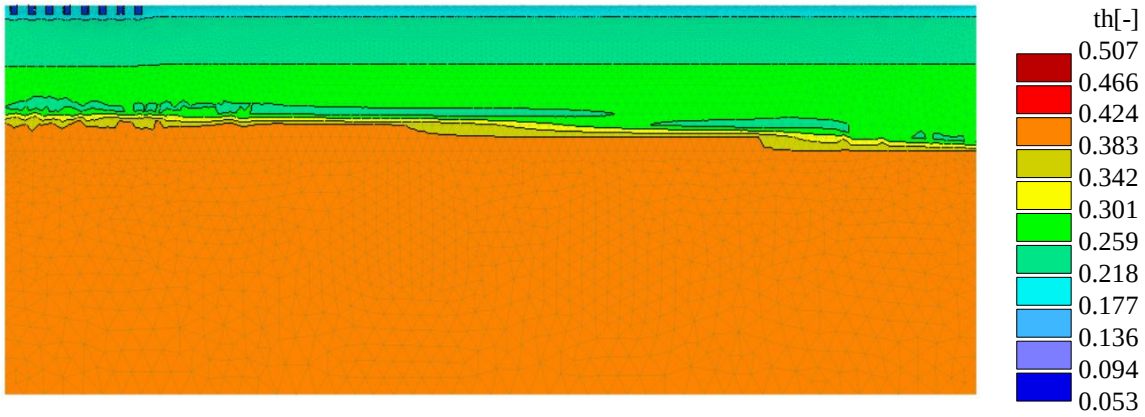

c)

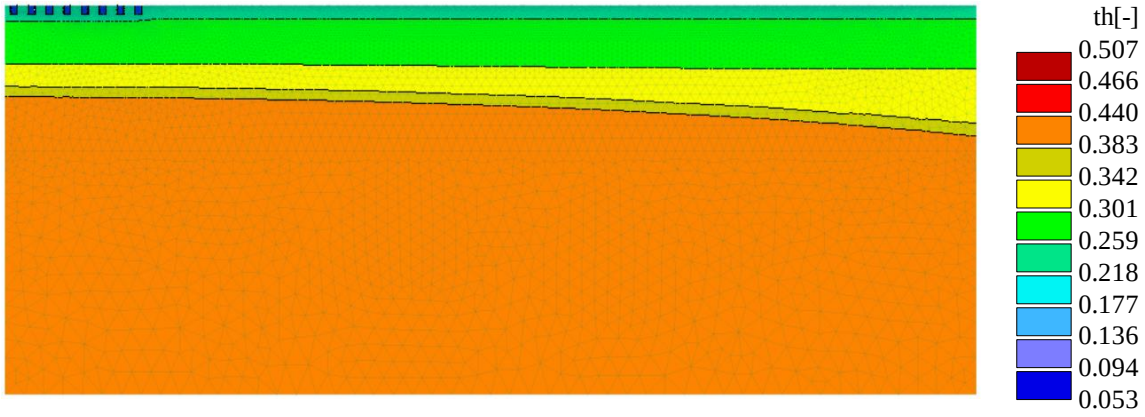

Figure 15. Water content values at end of dissipation simulations for a) loam, b) sandy loam, and c) silty loam. This figure shows the simulations for the existing trenches with a 15 m depth to WT.

3. RESULTS AND ANALYSIS

3.1. Effects of Changing the Water Table

The effects of modifying the water table on the cumulative surface infiltration were evaluated for the spacing tests and the dimensions tests. To represent these infiltration changes, differences in infiltration were calculated for 10 m to 15 m, 15 m to 20 m, and 10 m to 20 m water tables (Figures 16 and 17). For most loam and sandy loam simulations, infiltration increased as the WT changed from 10 m to 15 m, but decreased for 15 m to 20 m. Most silty loam simulations increased for both of these comparisons. The overall infiltration (10 m to 20 m WT) did often increase, but not for all for all values. These overall infiltration differences were also quite small (<0.3 m^2) for all of the simulations except for the sandy loam 10 m dimensions tests. This suggests that changing the depth to WT did not significantly affect the infiltration for all of the spacing and dimensions simulations (Figures 16 and 17) except for the one instance.

This decreased infiltration for the sandy loam 10 m WT dimensions tests can be explained from the local interference of the WT under the infiltration trenches. In these simulations, increasing the depth of the trenches while decreasing the width caused the wetting front from the gravel to reach the WT before the end of the inundation simulations (Figure 18). As a result, the specified pressure head at the surface was not able to lead to as much infiltration for the deeper and narrower trench geometries in the dimensions tests. This did not create any converge problems, as only a portion of the model domain had the WT connected to the surface.

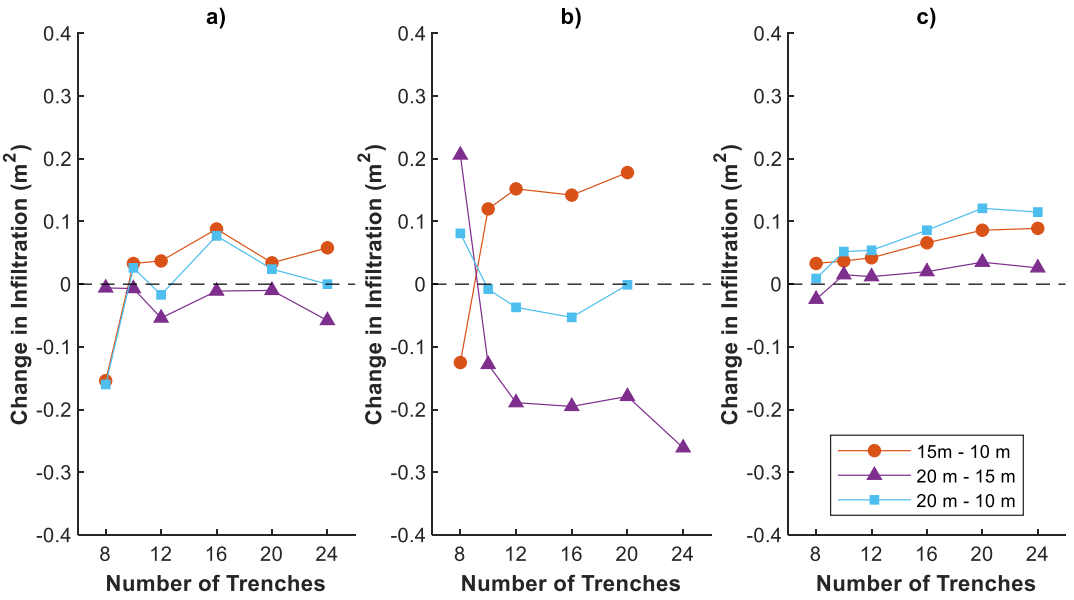

Figure 16. Infiltration differences for spacing tests for a) loam, b) sandy loam, and c) silty loam.

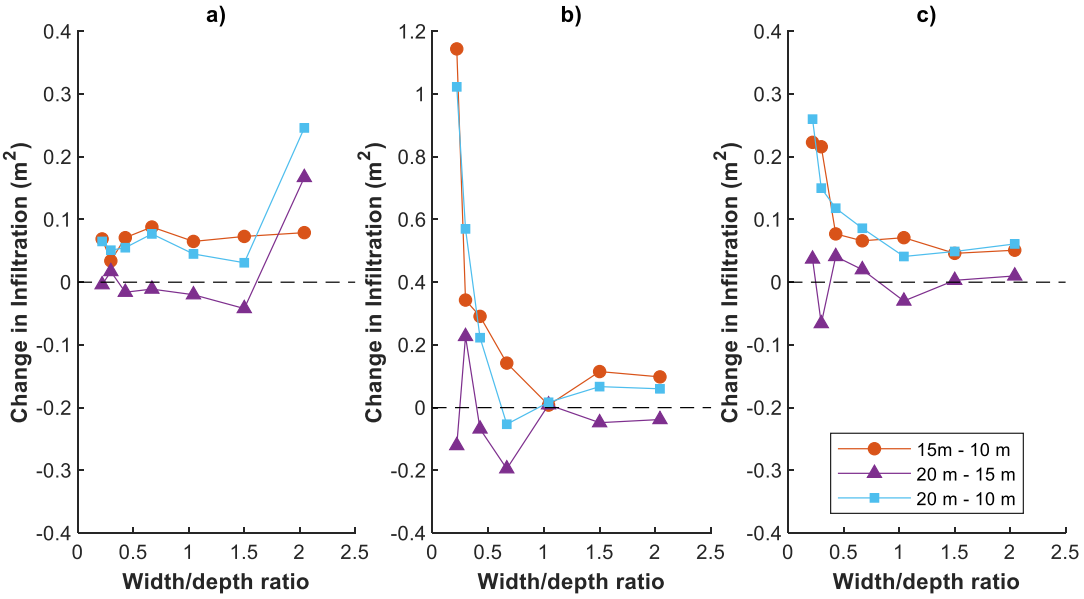

Figure 17. Infiltration differences for dimensions tests for a) loam, b) sandy loam, and c) silty loam.

a)

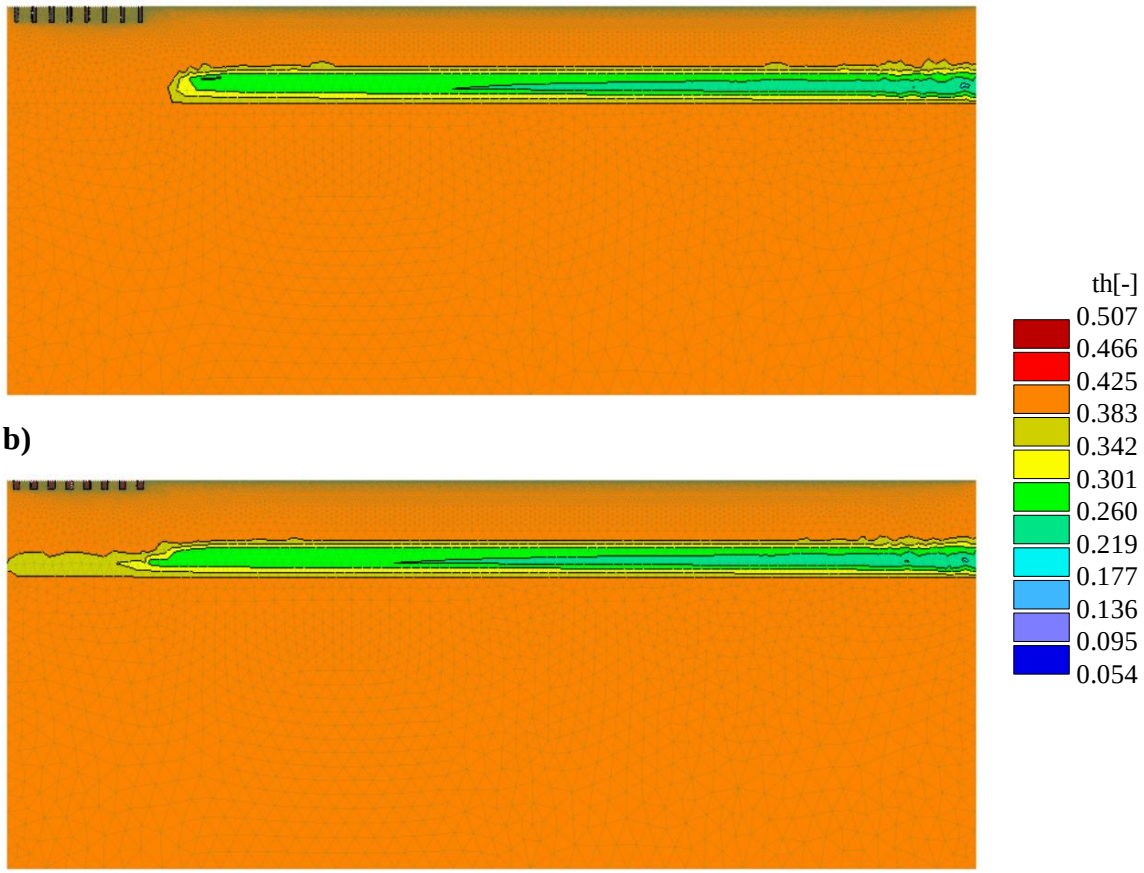

b)

Figure 18. Water content values at end of inundation simulations for the width/depth ratios of a) 0.2177 and b) 0.6667 (existing). This figure shows the simulations for the sandy loam soil type and a 10 m depth to WT.

If shallower depths to WT were tested, this would have more significantly affected the infiltration results. These shallower depths to WT were not tested due to software limitations that cause convergence problems when the full WT reaches the surface (as discussed in Section 2.4.1). Shallower WTs would also have also had both wetting fronts (under the trenches and under the existing soil) connect to the surface for some of the simulations, which would have created a fully saturated domain. If the

existing soil would already saturate the whole domain, there would also not be a significant need for MAR infiltration trenches.

3.2. Cumulative Surface Infiltration

The cumulative infiltration for the whole surface in the second and third simulation groups (Table 5) was summed to obtain the total cumulative infiltration. In order to isolate the impact of introducing the gravel trenches, these values were reduced by subtracting the total cumulative infiltration of the no gravel (control) simulations (shown in Table 7). The adjusted results are plotted in Figure 19 for the spacing tests and Figure 22 for the dimensions tests.

"Full gravel" simulations were also conducted in order to determine the maximum possible surface infiltration that could occur from increasing the number of trenches within the 15.24 m trench plot. The results from the full gravel simulations (Table 8) represent the upper limit of infiltration that is possible for the spacing tests and are the equivalent of 50 trenches within the trench plot. These values were also adjusted by subtracting out the no gravel (control) values (Table 7). It is important to note that the simulated infiltration does vary significantly for the different existing soils (Table 8), which is not evident if only looking at the adjusted values.

Table 7. No Gravel (Control) Simulation Results

Soil Type	Simulated Infiltration (m^2)		
	10 m depth to WT	15 m depth to WT	20 m depth to WT
Loam	35.46	35.44	35.45
Sandy Loam	90.39	91.84	92.08
Silty Loam	59.32	59.36	59.34

Table 8. Full Gravel Simulation Results

Soil Type	Adjusted Infiltration (m^2)		
	10 m depth to WT	15 m depth to WT	20 m depth to WT
Loam	7.70	7.75	7.76
Sandy Loam	8.71	8.89	8.98
Silty Loam	8.72	8.43	8.44

3.2.1. Cumulative Surface Infiltration: Spacing Tests

In the spacing tests, different numbers of trenches with a width of 0.6096 m and a depth of 0.9144 m were placed within the 15.24 m trench plot. These trenches have the same width and depth as the existing trenches (Albert et al., 2021), of which there are a total of 16. The adjusted results for each depth to WT show increasing infiltration that begins to slightly diminish as more trenches are added (Figure 19). However, these diminishing returns were less than initially anticipated for these simulated numbers of trenches.

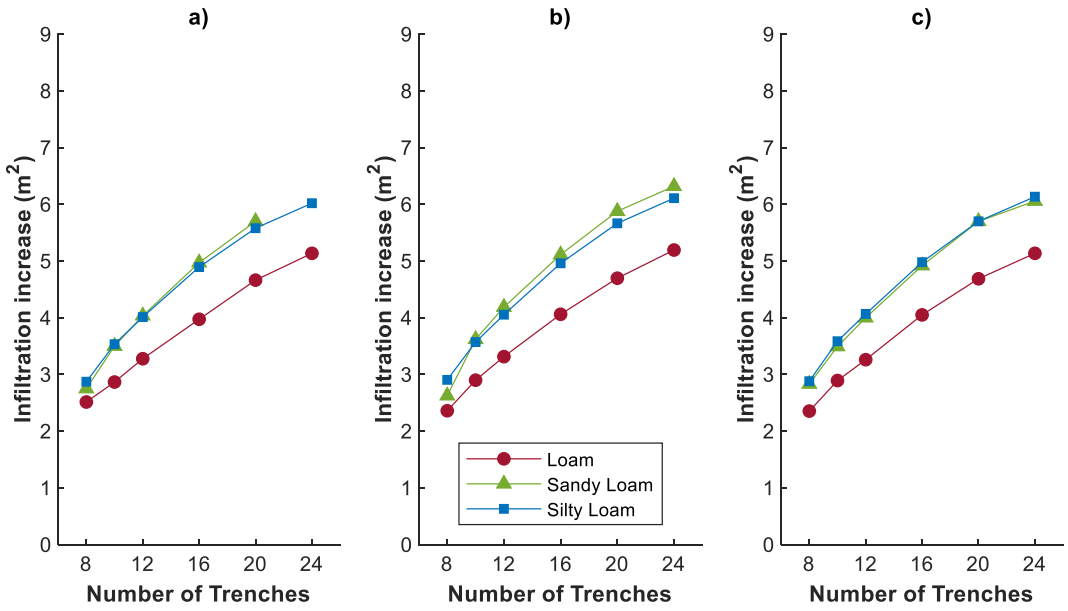

Figure 19. Increase in cumulative surface infiltration compared to control for a varied number of trenches within a 30.48 m plot. Simulations were conducted for depths to WT of a) 10 m, b) 15 m, and c) 20 m.

To obtain larger curves that better estimate the diminishing infiltration increases, the full gravel simulations were used. Since the full gravel simulations are the equivalent of 50 trenches with no spacing, this provided the upper limit of infiltration that could be obtained for each soil type. With this data point added, lines of best fit were calculated based upon the average infiltration for the three WTs (Figure 19). These lines of best fit are the second-degree polynomials that were obtained from the method of least squares. The polynomials in Figure 20 have the following equations:

$$Loam\ Infiltration = -0.0018N^2 + 0.2321N + 0.7334$$

$$Sandy\ Loam\ Infiltration = -0.0029N^2 + 0.3090N + 0.6634$$

$$Silty\ Loam\ Infiltration = -0.0027N^2 + 0.2887N + 0.9008$$

where *Infiltration* is the surface infiltration increase compared to the control simulations (m^2) and *N* is the number of trenches. The infiltration results were averaged for all three WTs in Figure 19 since the WT did not have a significant effect on infiltration for the spacing tests (as discussed in Section 3.1).

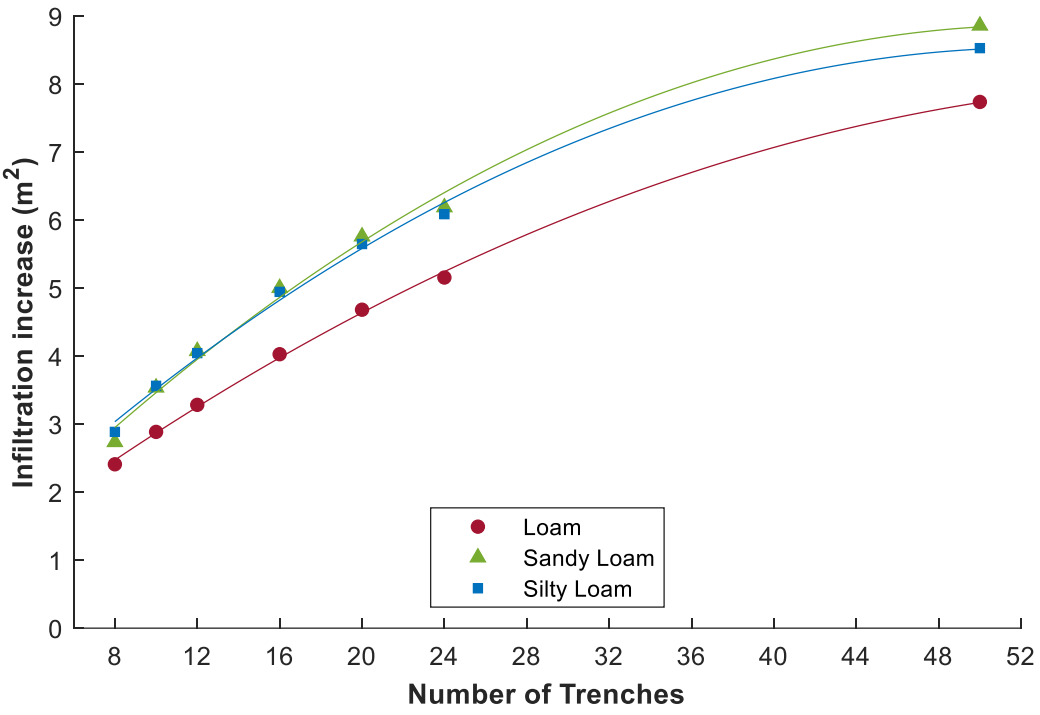

Figure 20. Average simulated infiltration values across all three WTs for the spacing tests. The lines of best fit are the second-degree polynomials obtained from method of least squares.

In Figure 21, the infiltration and number of trenches from Figure 20 are converted into dimensionless parameters in order to obtain values that are as general as possible. Infiltration was normalized by dividing the results from Figure 20 by the average of the 3 full gravel results for each soil type (Table 7) and multiplying by 100%. This accounted for the differences between the maximum infiltration limits for each soil

type. This ended up shifting the lines of best fit closer to each other in Figure 21 than in Figure 20, which showed a similar pattern across the three different soil types.

The number of trenches was also normalized by dividing this value by the maximum number of trenches (50) and multiplying by 100%. This is equivalent to the percentage of the 15.24 m trench plot that is covered in gravel, as the trenches all have the same dimensions. Figure 21 also plotted second-degree polynomial lines of best fit, which had the following equations:

$$Loam\ Percentage\ of\ Max\ Infiltration = -0.0060G^2 + 1.4999G + 9.4782$$

$$Sandy\ Loam\ Percentage\ of\ Max\ Infiltration = -0.0082G^2 + 1.7443G + 7.4885$$

$$Silty\ Loam\ Percentage\ of\ Max\ Infiltration = -0.0080G^2 + 1.6928G + 10.5623$$

where *Percentage of Max Infiltration* is the surface infiltration divided by the max infiltration and *G* is the percentage of gravel on the surface of the trench plot.

This conversion to dimensionless parameters allows for simple interpretation of Figure 21 without having to consider units. For example, the existing 16 trenches have 32% of the surface covered with gravel and about 52.1% of the max infiltration for loam. If the gravel cover were increased by 8%, this would increase the infiltration by 8.5% of the maximum value. However, an additional 8% increase in gravel cover would only increase infiltration by 6.1% of the maximum value.

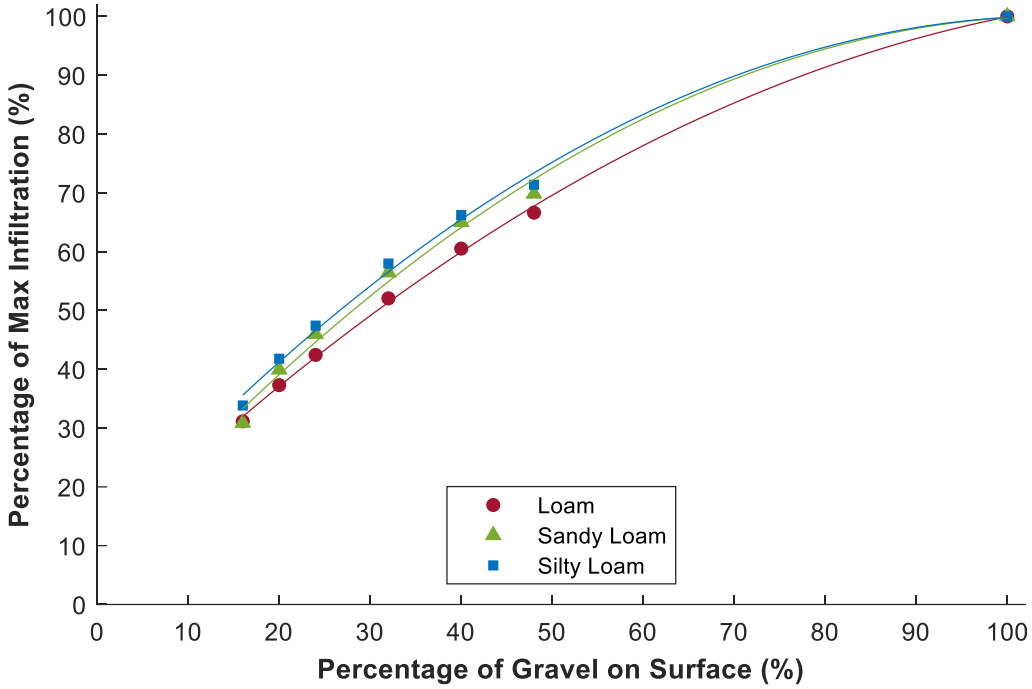

Figure 21. Dimensionless values and lines of best fit for the spacing tests results from Figure 20.

It is important to note that the percentage of max infiltration and percentage of gravel on the surface are not always weighted equally, as the relative importance of each variable depends upon the goals, economics, and characteristics of the site. These infiltration values were also determined using one specified trench width and depth. However, the polynomial lines of best fit can be used to roughly estimate how changing the number of trenches within an area will affect the infiltration.

3.2.2. Cumulative Surface Infiltration: Dimensions Tests

In the dimensions tests, the spacing and width of 16 infiltration trenches were varied within the 15.24 trench plot. The trenches maintained the same cross-sectional area and positions as the existing trenches (Albert et al., 2021), which have a spacing of

182.9 cm between the center lines of each trench. The adjusted results for each depth to WT show higher infiltration for deeper and narrower trenches than shallower and wider trenches for trenches with the same cross-sectional areas (Figure 22).

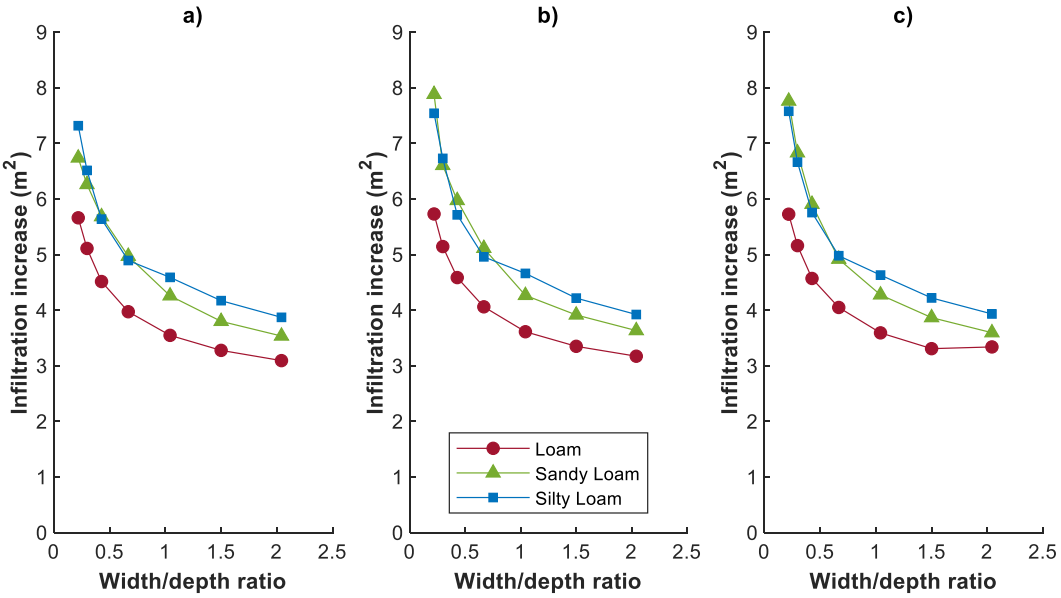

Figure 22. Increase in cumulative surface infiltration compared to control for varied trench width/trench depth ratios. Simulations were conducted for depths to WT of a) 10 m, b) 15 m, and c) 20 m.

Figure 23 shows the average values across the different WTs for the simulated values and also includes lines of best fit obtained with the method of least squares. Since the sandy loam 10 m WT simulations were the only simulations that were significantly affected by the WT interference, they were not included in the averaging. These lines of best fit are the reciprocal functions with the following equations:

$$Loam\ Infiltration = \frac{0.6187}{R} + 2.9877$$

$$Sandy\ Loam\ Infiltration = \frac{1.0157}{R} + 3.3036$$

$$Silty\ Loam\ Infiltration = \frac{0.8545}{R} + 3.6575$$

where *Infiltration* is the surface infiltration increase compared to the control simulations (m^2) and *R* is the ratio of the width of the trenches divided by the depth of the trenches.

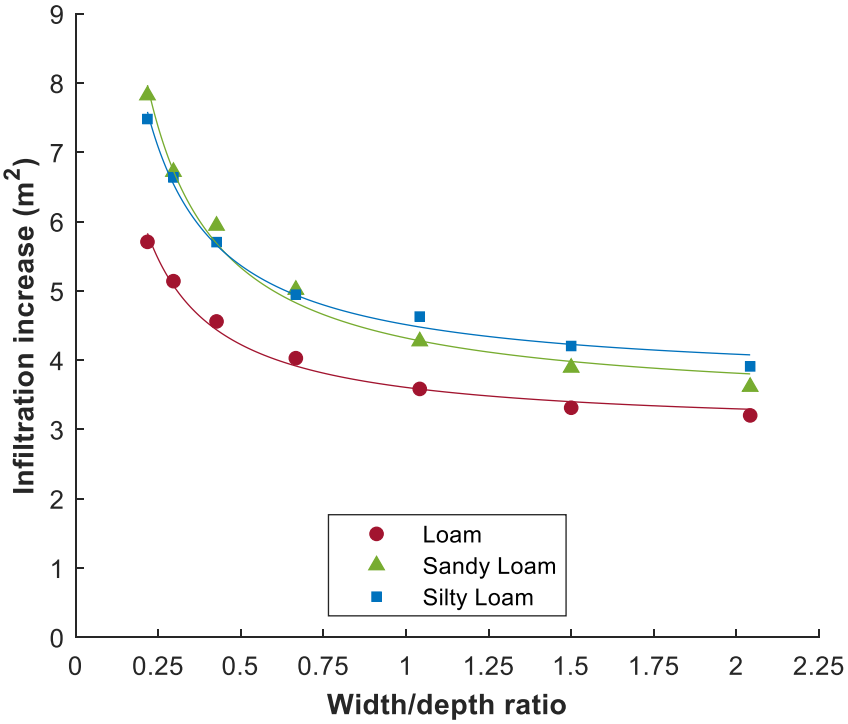

Figure 23. Average simulated infiltration values across all three WTs for the dimensions tests. The lines of best fit are the reciprocal functions obtained from the method of least squares.

Figures 22 and 23 show decreases in infiltration as width/depth ratio increases in a consistent pattern across the different soil types and WTs. The highest infiltration was simulated for the narrowest and deepest trenches in all of the dimensions simulations.

Infiltration was also much more sensitive to change for the lower width/depth ratios than the higher width/depth ratios.

The interference between trenches certainly impacted these infiltration results. Although the spacing between the trench centerlines was constant for the dimensions tests, narrower trenches meant more space between the edges of the trenches than wider trenches. By increasing the depth, this also created more infiltration space in the area below the trenches. As a result, interference between trenches is expected to be lower for deeper and narrower trenches than shallower and wider trenches.

3.3. Proportion of Bottom/Side Infiltration

The proportion of bottom and side infiltration leaving infiltration trenches was also measured in the spacing and dimensions simulations. This is measured as "bottom proportion," which is the amount of infiltration leaving the bottom of the trenches divided by the amount of infiltration leaving the bottom and sides of the trenches. The bottom proportions in Figures 24 and 25 showed consistent patterns across the different soil types and WTs, which suggests that these variables did not play a significant role here.

Fluxes were measured in HYDRUS for 3 different trenches in each simulation and then averaged to find each bottom proportion. 3 trenches were selected since HYDRUS allowed up to 10 mesh lines per simulation, and 3 lines were required per trench. The bottom proportion did decrease slightly for the trenches on the right end of the trench plot, as the flow coming from these trenches was less restricted from nearby

trenches. To account for these spatial differences, the 3 selected trenches included 1 on the left, 1 in the middle, and 1 on the right.

3.3.1. Proportion of Bottom/Side Infiltration: Spacing Tests

Figure 24 demonstrates that as additional trenches are added within the 15.24 m trench plot, the proportion of infiltration leaving the bottom of the trenches increases. This is due to the space between the trenches decreasing, which restricts the potential for lateral flow to occur.

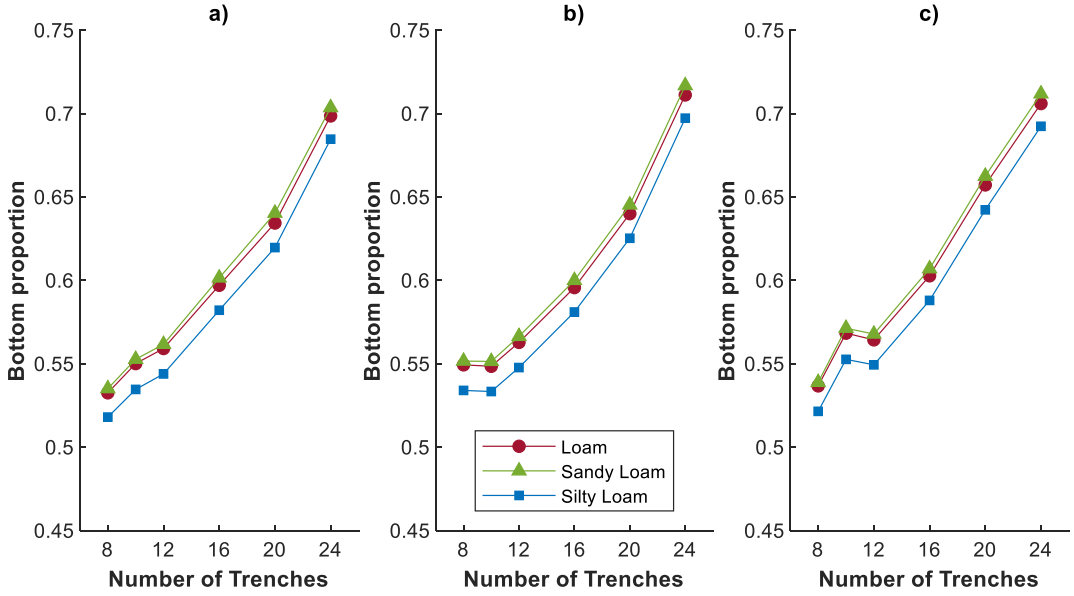

Figure 24. Proportion of cumulative infiltration leaving the bottom of the trenches compared to the bottom and the sides for a varied number of trenches within a 15.24 m plot. Simulations were conducted for depths to WT of a) 10 m, b) 15 m, and c) 20 m.

3.3.2. Proportion of Bottom/Side Infiltration: Dimensions Tests

Figure 25 shows that the bottom proportion also increases as the width/depth ratio increases. This is expected to occur, as there is a larger bottom width and a smaller side depth. However, the overall infiltration is also decreasing with this increasing

width/depth ratio (Figure 23). To show the actual bottom and side infiltration on one plot, the average bottom proportions for each soil type (Figure 25) are multiplied by these infiltration values for the spacing tests (Figure 23) to obtain Figure 26. Figure 26 shows that the infiltration coming from the bottom of the trenches does not significantly change as the width increases and the depth decreases. Instead, most of these infiltration changes are attributed to the side infiltration.

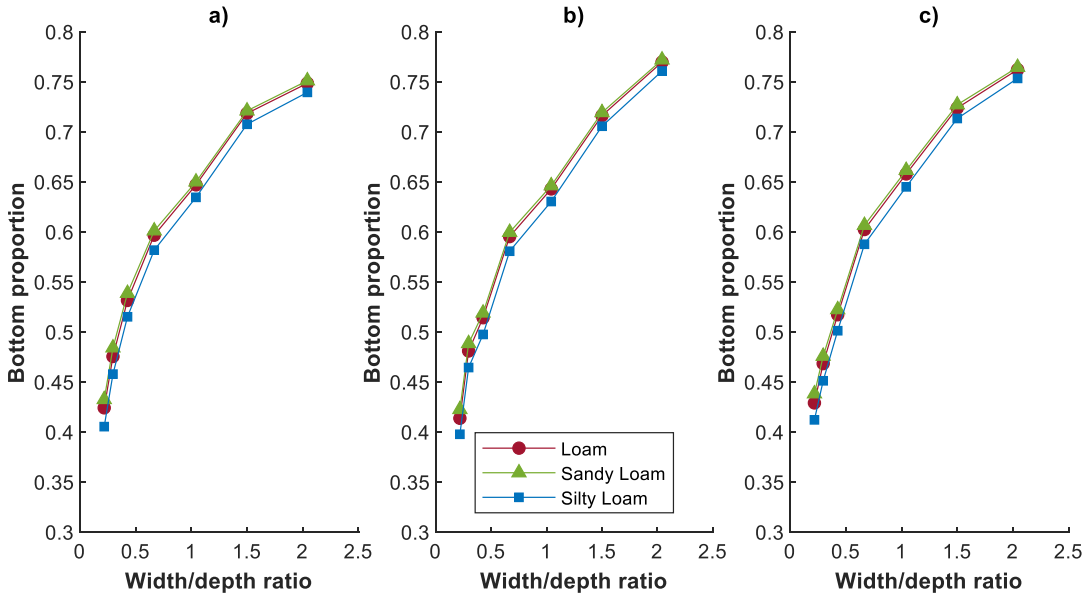

Figure 25. Proportion of cumulative infiltration coming from the bottom of the trenches divided by the proportion coming from the bottom and the sides for varied trench width/trench depth ratios. Simulations were conducted for depths to WT of a) 10 m, b) 15 m, and c) 20 m.

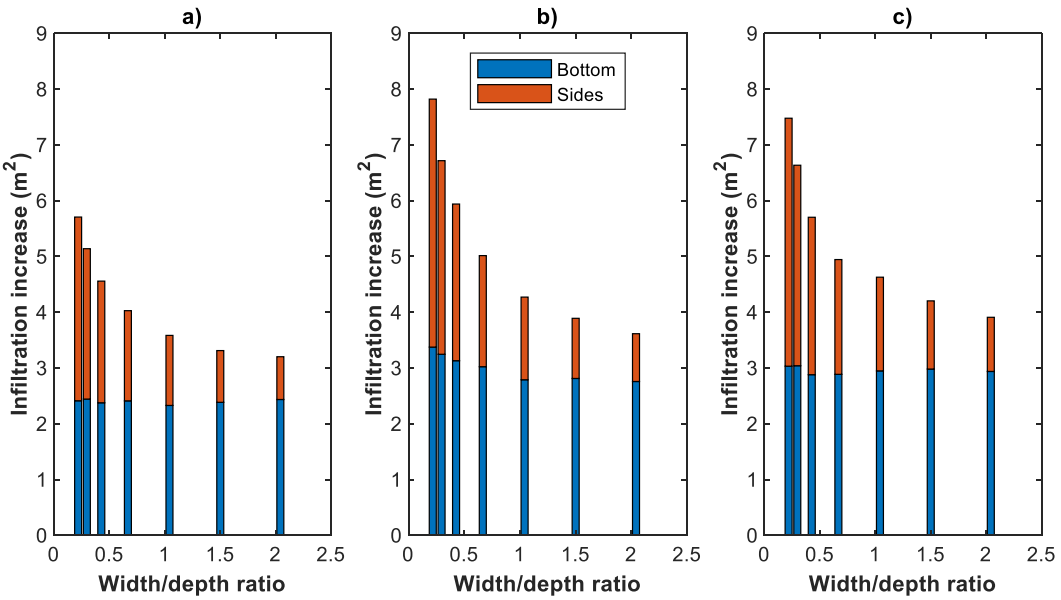

Figure 26. Amount of cumulative infiltration coming from the bottom and sides of the trenches for varied trench width/trench depth ratios. Simulations were conducted for a) loam, b) sandy loam, and c) silty loam using the average values of the three WTs.

3.4. Average Infiltration Rates

In the previous sections, infiltration was quantified as the added cumulative infiltration (in units of m^2) compared to the control plot for the whole domain. In this section, average infiltration rates for the trench plot section were estimated for the 48-hour inundation event (Tables 9, 10, and 11). To convert to infiltration rate, cumulative infiltration was divided by the horizontal length of the trench plot and divided by 2 days for the duration of the inundation event. The results were then averaged between the three simulated depths to WT.

Table 9. No Gravel and Full Gravel Average Infiltration Rates

Case	Average Simulated Infiltration Rate (m/d)		
	Loam	Sandy Loam	Silty Loam
No Gravel	0.177	0.458	0.296
Full Gravel	0.444	0.794	0.597

Table 10. Spacing Tests Average Infiltration Rates

Number of Trenches	Average Simulated Infiltration Rate (m/d)		
	Loam	Sandy Loam	Silty Loam
8	0.281	0.617	0.434
10	0.293	0.634	0.449
12	0.310	0.657	0.470
16	0.334	0.686	0.498
20	0.349	0.701	0.512
24	0.370	0.727	0.534

Table 11. Dimensions Tests Average Infiltration Rates

Width/Depth Ratio	Average Simulated Infiltration Rate (m/d)		
	Loam	Sandy Loam	Silty Loam
0.2177	0.396	0.780	0.593
0.2963	0.377	0.754	0.565
0.4267	0.354	0.719	0.529
0.6667	0.334	0.686	0.498
1.0417	0.317	0.657	0.474
1.5000	0.306	0.637	0.457
2.0417	0.299	0.623	0.444

4. CONCLUSIONS

4.1. Summary of the Findings

In this study, the spacing, width, and depth of infiltration trenches were compared for three soil types and three WT depths to determine the resulting infiltration rates. Functions were determined for each soil type that describe these infiltration changes for the spacing and dimensions tests.

Trench spacing was modified by changing the number of trenches within the 15.24 m trench plot and maintaining the same dimensions. Modeling results for the spacing tests showed that infiltration increased as additional trenches were added, but there were diminishing returns. The proportion of infiltration coming from the bottom of the trenches increased as additional trenches were added in the spacing tests.

The width and depth were varied inversely while maintaining a constant trench volume and the same number of trenches. Modeling results for the dimensions tests showed higher infiltration for deep and narrow trenches than shallow and wide trenches. This infiltration increase for deep and narrow trenches was came mostly from infiltration from the side of the trenches. Infiltration coming from the bottom of the trenches stayed relatively constant as the width and depth of the trenches were modified.

4.2. Directions for Future Research

Numerical modeling of clogging in multiple trench systems would be useful for determining how to best size infiltration trenches. Clogging should especially be considered for MAR projects that use stormwater due to the associated sedimentation.

Pretreatment and scheduled operation and maintenance of the trench systems can also be considered in the modeling to reduce the amount of clogging.

Modeling of multi-trench systems could be conducted for longer time periods, which could include a variety of inundation and precipitation events. Evaluating over a longer time period may also show diminishing infiltration from the impacts of high initial water tables and water contents. Introducing different pressure head values at the surface may also impact the infiltration performance of the trenches.

Future MAR numerical modeling based in detention basins could incorporate the ground slope of the basin into the model. This would account for the fact that not all of the trenches receive water from smaller storms, which affects the performance of the system.

REFERENCES

Akan, A. O. (2002). Sizing stormwater infiltration structures. *Journal of Hydraulic Engineering*, *128*(5), 534–537. https://doi.org/10.1061/(asce)0733-9429(2002)128:5(534)

Albert, S., Miller, G. R., Majumdar, S., & Chen, L. (2021). "Drainage Reuse Initiative: Phase II" for the Harris County Flood Control District and the Harris County Precinct 4 Commissioner's Office.

Baveye, P., Vandevivere, P., Hoyle, B. L., DeLeo, P. C., & de Lozada, D. S. (1998). Environmental impact and mechanisms of the biological clogging of saturated soils and aquifer materials. *Critical Reviews in Environmental Science and Technology*, *28*(2), 123–191. https://doi.org/10.1080/10643389891254197

Błażejewski, R., Nieć, J., Murat-Błażejewska, S., & Zawadzki, P. (2018). Comparison of infiltration models with regard to design of rectangular infiltration trenches. *Hydrological Sciences Journal*, *63*(11), 1707–1716. https://doi.org/10.1080/02626667.2018.1523616

Bouwer, H. (2002). Artificial recharge of groundwater: Hydrogeology and engineering. *Hydrogeology Journal*, *10*(1), 121–142. https://doi.org/10.1007/s10040-001-0182-4

Braun, C. L., & Ramage, J. K. (2020). Status of groundwater-level altitudes and long-term groundwater-level changes in the Chicot, Evangeline, and Jasper Aquifers, Houston-galveston region, Texas, 2020. *Scientific Investigations Report*. https://doi.org/10.3133/sir20205089

Cai, W., Santoso, A., Wang, G., Yeh, S.-W., An, S.-I., Cobb, K. M., Collins, M., Guilyardi, E., Jin, F.-F., Kug, J.-S., Lengaigne, M., McPhaden, M. J., Takahashi, K., Timmermann, A., Vecchi, G., Watanabe, M., & Wu, L. (2015). Enso and Greenhouse Warming. *Nature Climate Change*, *5*(9), 849–859. https://doi.org/10.1038/nclimate2743

Campisano, A., Creaco, E., & Modica, C. (2011). A simplified approach for the design of infiltration trenches. *Water Science and Technology*, *64*(6), 1362–1367. https://doi.org/10.2166/wst.2011.170

Chahar, B. R., Graillot, D., & Gaur, S. (2012). Storm-water management through infiltration trenches. *Journal of Irrigation and Drainage Engineering*, *138*(3), 274–281. https://doi.org/10.1061/(asce)ir.1943-4774.0000408

Cleaveland, M. K., Banner, J. L., Casteel, R. C., Stahle, D. K., & Votteler, T. H. (2011). Extended Chronology of Drought in South Central, Southeastern, and West Texas. *Texas Water Journal*, *2*(1), 54–96. https://doi.org/10.21423/twj.v2i1.2049

Cook, B. I., Seager, R., Williams, A. P., Puma, M. J., McDermid, S., Kelley, M., & Nazarenko, L. (2019). Climate change amplification of natural drought variability: The historic mid-twentieth-century North American drought in a warmer world. *Journal of Climate*, *32*(17), 5417–5436. https://doi.org/10.1175/jcli-d-18-0832.1

Coplin, L. S., & Galloway, D. (1999) Houston-Galveston, Texas: Managing coastal subsidence. In Land subsidence in the United States: *US Geological Survey Circular 1182*, 35–48.

Duchene, M., McBean, E. A., & Thomson, N. R. (1994). Modeling of Infiltration from Trenches for Storm-Water Control. *Journal of Water Resources Planning and Management*, *120*(3), 276–293.

Emanuel, K. (2017). Assessing the present and future probability of Hurricane Harvey's rainfall. *Proceedings of the National Academy of Sciences*, *114*(48), 12681–12684. https://doi.org/10.1073/pnas.1716222114

Fetter, C. W. (2018). *Applied Hydrogeology* (4th ed.). Waveland press.

Finch, S. D., Radcliffe, D. E., & West, L. T. (2008). Modeling trench sidewall and bottom flow in on-site wastewater systems. *Journal of Hydrologic Engineering*, *13*(8), 693–701. https://doi.org/10.1061/(asce)1084-0699(2008)13:8(693)

Gergis, J. L., & Fowler, A. M. (2006). How unusual was late 20th century El Niño-Southern Oscillation (ENSO)? Assessing evidence from tree-ring, coral, ice-core and documentary palaeoarchives, A.D. 1525-2002. *Advances in Geosciences*, *6*, 173–179. https://doi.org/10.5194/adgeo-6-173-2006

Gershunov, A. (1998). Enso influence on intraseasonal extreme rainfall and temperature frequencies in the contiguous United States: Implications for long-range predictability. *Journal of Climate*, *11*(12), 3192–3203. https://doi.org/10.1175/1520-0442(1998)011%3C3192:EIOIER%3E2.0.CO;2

Guo, Y., & Gao, T. (2016). Analytical equations for estimating the total runoff reduction efficiency of infiltration trenches. *Journal of Sustainable Water in the Built Environment*, *2*(3). https://doi.org/10.1061/jswbay.0000809

Heilweil, V. M., Benoit, J., & Healy, R. W. (2015). Variably saturated groundwater modelling for optimizing managed aquifer recharge using trench infiltration. *Hydrological Processes*, *29*(13), 3010–3019. https://doi.org/10.1002/hyp.10413

Indrawan, I. G. B., Rahardjo, H., & Leong, E. C. (2006). Effects of coarse-grained materials on properties of residual soil. *Engineering Geology*, *82*(3), 154–164. https://doi.org/10.1016/j.enggeo.2005.10.003

Kasmarek, M. C. (2013). Hydrogeology and Simulation of Groundwater Flow and Land-Surface Subsidence in the Northern Part of the Gulf Coast Aquifer System, Texas, 1891-2009 (Version 1.1). U.S. Geological Survey Scientific Investigations Report 2012-5154. https://doi.org/10.3133/sir20125154

Kasmarek, M. C., & Robinson, J. L. (2004). Hydrogeology and simulation of ground-water flow and land-surface subsidence in the northern part of the Gulf Coast Aquifer System, Texas. U.S. Geological Survey Scientific Investigations Report 2004-5102. https://doi.org/10.3133/sir20045102

Kearns, T. J., Wang, G., Bao, Y., Jiang, J., & Lee, D. (2015). Current land subsidence and groundwater level changes in the Houston Metropolitan Area (2005–2012). *Journal of Surveying Engineering*, *141*(4). https://doi.org/10.1061/(asce)su.1943-5428.0000147

Kurtzman, D., & Scanlon, B. R. (2007). El Niño-Southern Oscillation and Pacific decadal oscillation impacts on precipitation in the southern and central United States: Evaluation of spatial distribution and predictions. *Water Resources Research*, *43*(10). https://doi.org/10.1029/2007wr005863

Lindsey, G., Roberts, L., & Page, W. (1992). Inspection and maintenance of infiltration facilities. *Journal of Soil and Water Conservation*, *47*(6), 481–486.

Locatelli, L., Mark, O., Mikkelsen, P. S., Arnbjerg-Nielsen, K., Wong, T., & Binning, P. J. (2015). Determining the extent of groundwater interference on the performance of infiltration trenches. *Journal of Hydrology*, *529*, 1360–1372. https://doi.org/10.1016/j.jhydrol.2015.08.047

Maliva, R. G. (2020). *Anthropogenic aquifer recharge: WSP methods in Water Resources Evaluation Series No. 5*. Springer.

Maniquiz-Redillas, M. C., Geronimo, F. K., & Kim, L.-H. (2014). Investigation on the effectiveness of Pretreatment in Stormwater Management Technologies. *Journal of Environmental Sciences*, *26*(9), 1824–1830. https://doi.org/10.1016/j.jes.2014.06.018

Miller, M. M., & Shirzaei, M. (2019). Land subsidence in Houston correlated with flooding from Hurricane harvey. *Remote Sensing of Environment*, *225*, 368–378. https://doi.org/10.1016/j.rse.2019.03.022

Mualem, Y. (1976). A new model for predicting the hydraulic conductivity of unsaturated porous media. *Water Resources Research*, *12*(3), 513–522. https://doi.org/10.1029/wr012i003p00513

Natural Resources Conservation Service, United States Department of Agriculture. (2022). Web Soil Survey. Retrieved from http://websoilsurvey.sc.egov.usda.gov/

Nielsen-Gammon, J. W., Banner, J. L., Cook, B. I., Tremaine, D. M., Wong, C. I., Mace, R. E., Gao, H., Yang, Z. L., Gonzalez, M. F., Hoffpauir, R., Gooch, T., & Kloesel, K. (2020). Unprecedented drought challenges for Texas Water Resources in a changing climate: What do researchers and stakeholders need to know? *Earth's Future*, *8*(8). https://doi.org/10.1029/2020ef001552

NOAA National Centers for Environmental Information (NCEI). (2022). *U.S. billion-dollar weather and climate disasters*. Retrieved from https://www.ncei.noaa.gov/access/billions/

Schaap, M. G., Leij, F. J., & van Genuchten, M. T. (2001). ROSETTA: A computer program for estimating soil hydraulic parameters with hierarchical pedotransfer functions. *Journal of Hydrology*, *251*(3-4), 163–176. https://doi.org/10.1016/s0022-1694(01)00466-8

Schueler, T. K. (1987). Controlling Urban Runoff: A Practical Manual for Planning and Designing Urban BMPs. Publication #87703 of the Washington Metropolitan Council of Governments.

Šejna, M, Šimůnek, J., & van Genuchten, M. T. (2014). The HYDRUS software package for simulating two-and three-dimensional movement of water, heat, and multiple solutes in variably-saturated media. *User Manual, Version 2.4*.

Šimůnek, J. (2002). runoff simulation difference between Hydrus 1d and 2d [web log]. PC-Progress Discussion Forums. Retrieved from https://www.pc-progress.com/forum/viewtopic.php?f=3&t=3982

Šimůnek, J. (2006). Gravel Van Genuchten parameters [web log]. PC-Progress Discussion Forums. Retrieved from https://www.pc-progress.com/forum/viewtopic.php?f=4&t=625.

Šimůnek, J., & Šejna, M. (2009). Notes on Spatial and Temporal Discretization. Retrieved from https://www.pc-progress.com/Images/Pgm_Hydrus3D2/Notes_on_Spatial_and_Temporal_Discretization.pdf

Šimůnek, J., van Genuchten, M. T., & Šejna, M. (2020). The HYDRUS software package for simulating two-and three-dimensional movement of water, heat, and multiple solutes in variably-saturated media. *Technical Manual, Version 3.03*.

Siriwardene, N., Deletic, A., & Fletcher, T. (2007). Clogging of stormwater gravel infiltration systems and filters: Insights from a laboratory study. *Water Research*, *41*(7), 1433–1440. https://doi.org/10.1016/j.watres.2006.12.040

Smith, W. B., Miller, G. R., & Sheng, Z. (2017). Assessing aquifer storage and recovery feasibility in the Gulf Coastal Plains of Texas. *Journal of Hydrology: Regional Studies*, *14*, 92–108. https://doi.org/10.1016/j.ejrh.2017.10.007

Texas Water Development Board. (2022). *2022 State Water Plan*. Retrieved from http://www.twdb.texas.gov/waterplanning/swp/2022/

van Genuchten, M.Th. (1980). A closed-form equation for predicting the hydraulic conductivity of unsaturated soils. *Soil Science Society of America Journal*. 44, 892–898

Virginia Department of Transportation. (2013). BMP Design Manual of Practice. Retrieved from https://virginiadot.org/business/locdes/bmp_designmanual.asp

Wang, J., & Guo, Y. (2020). Proper sizing of infiltration trenches using closed-form analytical equations. *Water Resources Management*, *34*(12), 3809–3821. https://doi.org/10.1007/s11269-020-02645-x

Wijaya, M., Leong, E. C., & Rahardjo, H. (2015). Effect of shrinkage on air-entry value of soils. *Soils and Foundations*, *55*(1), 166–180. https://doi.org/10.1016/j.sandf.2014.12.013

Zhang, W., Villarini, G., Vecchi, G. A., & Smith, J. A. (2018). Urbanization exacerbated the rainfall and flooding caused by Hurricane Harvey in Houston. *Nature*, *563*(7731), 384–388. https://doi.org/10.1038/s41586-018-0676-z